Optical Tweezers: A Comprehensive Tutorial from Calibration to Applications

JAN GIESELER,[1,2] JUAN RUBEN GOMEZ-SOLANO,[3] ALESSANDRO MAGAZZÙ,[4,5] ISAAC PÉREZ CASTILLO,[3] LAURA PÉREZ GARCÍA,[5] MARTA GIRONELLA-TORRENT,[6] XAVIER VIADER-GODOY,[6] FELIX RITORT,[6] ALEJANDRO V. ARZOLA,[3] KAREN VOLKE-SEPULVEDA,[3] AND GIOVANNI VOLPE[5,*]

[1] *ICFO - Institut de Ciències Fotòniques, The Barcelona Institute of Science and Technology, 08860 Castelldefels (Barcelona), Spain*
[2] *Harvard University, Department of Physics, 17 Oxford St., Cambridge, MA, USA*
[3] *Instituto de F´sica, Universidad Nacional Autónoma de México, Apdo. Postal 20-364, 01000Cd. México, Mexico.*
[4] *MagoLab, Gothenburg, Sweden*
[5] *Department of Physics, University of Gothenburg, 41296 Gothenburg, Sweden.*
[6] *Small Biosystems Lab, Departament de Fsica de la Matèria Condensada, Facultat de Física, Universitat de Barcelona, 08028 Barcelona, Spain*
[*] *giovanni.volpe@physics.gu.se*

Abstract: *...*

Contents

1. Calibration

As we have seen in section **??**, *an optical trap acts as a microscopic Hookeian spring with a fixed stiffness so that the restoring force is proportional to the displacement of the optically trapped particle from the center of the optical trap. The calibration of an optical tweezers entails the determination of the value of the optical trap stiffness, which in general depends both on the properties of the light beam and on the optically trapped particle. The calibration of an optical tweezers is thus essential in order to be able to use it as a microscopic force transducer, i.e., to measure and exert forces in the femtonewton and piconewton range. In principle, it should be possible to determine the value of the stiffness for a given experimental configuration where the properties of the focused laser beam and the optically trapped particles are known. In fact, this has been done in certain cases [1]. However, this is in general a cumbersome task because an exact description of the focused beam and its interaction with particles depend on several parameters which are very difficult to know accurately and may vary drastically even in the same experiment. For example,*

Notation	Explanation
$x_\ell \equiv x(t_\ell)$	position of particle at time $t_\ell = \ell \Delta t$
$\{x_\ell^{(m)}\}_{\ell=1}^{N}$	recorded time series of particle's position during the m-th experiment with N samples
$\{\hat{x}_\ell^{(m)}\}_{\ell=1}^{L}$	uncorrelated time series at time intervals $\ell\widehat{\Delta t}$ with $\widehat{\Delta t} = r\Delta t$ and r an integer
$\kappa_x^{(\mathrm{ex})}$	experimental estimate of the trap stiffness
$\tau_x^{(\mathrm{ex})}$	experimental estimate of characteristic relaxation time
$D^{(\mathrm{ex})}$, $D^{(\mathrm{th})}$	experimental estimate and theoretical value of diffusion constant
$\gamma^{(\mathrm{ex})}$, $\gamma^{(\mathrm{th})}$	experimental estimate and theoretical value of friction coefficient
T_s	Total aquisition time for each experiment m

Table 1. Notation used in the explanation of calibration techniques.

just the theoretical description of the focused beam requires precise information of the focusing lens, the thickness of the coverslip, the refractive index of the media and their light absorption and the position of the focus inside the sample, which are all difficult to obtain. Moreover, even with all this information at hand, the interaction between a focused beam and a trapped object is very complex, requiring to solve a computationally intensive electromagnetic scattering problem [2]. Therefore, the development and improvement of in-situ calibration methods have been very important to extend the practical applications of optical tweezers.

From a practical point of view, this idea relies on the ability to determine the stiffness of the optical tweezers from the dynamics of a trapped particle with high accuracy and speed. The calibration methods can be classified as either passive or active, depending on the configuration of the experiment. Passive methods (sections from 1.2 to 1.10) require that the optical tweezers remains static, and all the information of the trap will be indirectly extracted from the Brownian trajectory of the trapped particle building on some physical assumptions. In contrast, during active calibration (section 1.11), the trapped particle is forced to move periodically by a known time-dependent perturbation, which may be exerted either by an external force, as the one generated by a periodic movement of the sample cell, or by a periodic movement of the position of the optical tweezers. Recently, some techniques have been developed to extract the force exerted by an optical tweezers directly from the recording on a CCD (CMOS), or on a photodiode, of the scattered light of the trapping beam [3] (section x.x). These techniques have their own capabilities and range of applicability and in some cases they may bring complementary information about the problem.

Using some real data acquired by these approaches, in this section we will review the concepts and procedures commonly used to analyze the data and infer properties of the optical trap and the particle. Based on the sampling of the particle's trajectory there is a wide range of methods that can be used to infer properties of the trap, including the ones of the fluid and the particle itself. These include: the potential method (section 1.2), the equipartition method (section 1.3), the mean squared displacement (MSD) analysis (section 1.4), autocorrelation function (ACF) analysis (section 1.5), power spectrum density (PSD) analysis (section 1.6), the drift method (section 1.7), the force reconstruction via maximum-likelihood-estimator analysis (FORMA) (section 1.8), Bayesian inference (section 1.9), measurement of non-conservative force

Parameter	**Value**
Particle	Polystyrene particle with radius $a = 1.03 \pm XX$ μm
Laboratory temperature	$T = 20°\text{C}$ ($T = 293.15\,\text{K}$)
Sampling frequency	$f_s = 10^5$ Hz
Time interval	$\Delta t = \frac{1}{f_s} = 10^{-5}$ s
viscosity of water at lab temperature	$\eta = 1.00$ mPa s
friction coefficient (by Stokes' formula (1))	$\gamma^{(\text{th})} = 19.4 \pm XX$ pN ms μm^{-1}
diffusion coefficient (by Einstein's formula (2))	$D^{(\text{th})} = 0.208627 \pm XX$ μm^2 s^{-1}
total number of experiments	$M = 5$
total number data points at each experiment	$N = 10^6$
objective lens	Olympus UPLSAPO 60X 1.2 NA water immersion REVISAR
laser wavelength	1064 nm
Laser power at the sample for experiment I, II and III	2.3mW, 6.0mW, and 9.2mW

Table 2. Experimental parameters. A microscopic particle immersed in water is trapped with a tightly-focused laser beam in an standard optical tweezers configuration, and tracked using a quadrant photodiode. Three different stiffness, depending on the laser power, are explored to illustrate the proper working of the calibration methods.

fields (section 1.10), and active calibration techniques (section 1.11). Moreover, there exists other approaches that allow us to infer directly optical forces, which we will briefly also discussed (section 1.12). To illustrate in a practical way the use of all the calibration methods, with all their nuances, we have carried out a series of standard experiments, whose details can be found in Table 2. These datasets are provided as additional materials for the reader to be able to reproduce the results we present and to practice the use of the various calibration techniques. Moreover, we also provide the implementation in Matlab of the calibration techniques explained in this section. An overview and comparison of the various calibration methods can be found in Table 3 and the results obtained on the test datasets in Table 4. A summary of the notation used in this section together with an explanation can be found in Table 1. Most of the mathematical details regarding the non-linear fitting, and so on, have been relegated to section 1.13.

1.1. Time series acquisition and notation

In the simplest form, a particle trapped in an optical tweezer is modeled as a Brownian particle in an harmonic potential. Here, we consider the overdamped regime, where the inertia of the particle is neglected, which, more often than not, corresponds to the range of experimental parameters for standard experiments and, moreover, is at this the regime at which most of the calibration techniques explained below apply. For sake of clarity, we consider a spherical particle of radius a immersed in a fluid with viscosity η at an absolute temperature T. According to Stokes' law, the friction coefficient is given by:

$$\gamma = 6\pi\eta a\,, \tag{1}$$

while the diffusion constant is given by the Einstein-Smoluchowski relation

$$D = \frac{k_{\mathrm{B}}T}{\gamma}\,, \tag{2}$$

where $k_{\mathrm{B}} = 1.3806 \cdot 10^{-5}\,\mathrm{pN}\,\mu\mathrm{m}\,\mathrm{K}^{-1}$ is Boltzmann's constant. The trajectory $x(t)$ of an overdamped Brownian particle is described by the Langevin equation

$$\frac{dx(t)}{dt} = \frac{1}{\gamma}F(x) + \sqrt{2D}W_x(t)\,, \tag{3}$$

where $F(x)$ is a deterministic force exerted on the particle (in our case the optical force) and $W_x(t)$ is a white noise with zero mean and Dirac-delta-correlated variance, i.e., $\langle W_x(t)W_x(t')\rangle = \delta(t-t')$.
Using some of the experimental setups described in this tutorial, we proceed to record the particle's position $x_\ell \equiv x(t_\ell)$ at times $t_\ell = \ell\Delta t$ with $\ell = 1,\ldots,N$, which yields a time series $\{x_\ell\}_{\ell=1}^{N}$ for a single trajectory. In order to provide estimates with error bars to the properties of the optical trap and that of the particle one has two choices: one can either repeat the experiment M times or to divide the time series of a single experiment of size S into M blocks of $N = S/M$ data points each. Either way, we end up with a set of times series $\{x_\ell^{(m)}\}_{\ell=1}^{N}$ for $m = 1,\ldots,M$.

1.2. Potential analysis

For a conservative force (which is always true in one dimension), $F(x) = -\frac{dU(x)}{dx}$ and the probability density of finding the particle at a given position x at thermal equilibrium follows the Maxwell-Boltzmann distribution:

$$\rho(x) = \rho_0 e^{-\frac{U(x)}{k_{\mathrm{B}}T}}\,, \tag{4}$$

where ρ_0 is a normalization factor ensuring that $\int \rho(x)dx = 1$. The potential $U(x)$ can then be reconstructed as

$$U(x) = -k_{\mathrm{B}}T \ln\frac{\rho(x)}{\rho_0}\,. \tag{5}$$

The expression in equation (4) is an equilibrium distribution that theoretically corresponds to the probability of finding a particle from an ensemble of independent particles, at a given position x. However, in practice, this distribution is usually computed from data sets coming from the trajectory of a particle, consisting of data points not necessarily uncorrelated. For instance for a harmonic potential $U(x) = \frac{\kappa_x}{2}(x - x_{eq})^2$, there exists a characteristic relaxation time $\tau_{\mathrm{ot},x} = \gamma/\kappa_x$ so that two arbitrary points along the trajectory $x(t)$ and $x(t')$ are uncorrelated if $|t-t'| \gg \tau_{\mathrm{ot},x}$ [4]. This means that we need to work in a regime in which $T_s \gg \Delta t \gg \tau_{\mathrm{ot},x}$, where the first condition implies that we have enough samples and the second one that the time series is uncorrelated.
Assuming that we have an uncorrelated time series $\{\hat{x}_\ell^{(m)}\}_{\ell=1}^{N}$, we first seek a common maximum and minimum values of the position variable, denoted x_{max} and x_{min}, respectively. To construct the empirical distribution $\rho_m^{(\mathrm{ex})}\left(x;\{\hat{x}_\ell^{(m)}\}_{\ell=1}^{N}\right)$ of $\rho(x)$ for the time series $m = 1,\ldots M$, we discretize the interval $[x_{min}, x_{max}]$ as:

$$x_\alpha = x_{min} + \frac{\alpha}{P}(x_{max} - x_{min}), \quad \alpha = 0,1,\ldots,P-1 \tag{6}$$

so that the empirical distribution consists of a histogram of P bins. We then use the m-th time series to calculate the frequency of data points falling in each subinterval. Once we have obtained the normalized

histogram of P bins for the M experiments, we have a list of estimates $\{\rho_m^{(\mathrm{ex})}(x_\alpha)\}_{m=1}^{M}$ *for* $\rho(x)$*, from which we obtain its empirical mean value and variance, viz.*

$$\overline{\rho^{(\mathrm{ex})}}(x_\alpha) = \frac{1}{M}\sum_{m=1}^{M}\rho_m^{(\mathrm{ex})}(x_\alpha)\,, \quad [\sigma_\alpha^{(\rho)}]^2 = \frac{1}{M-1}\sum_{m=1}^{M}\left[\rho_m^{(\mathrm{ex})}(x_\alpha) - \overline{\rho^{(\mathrm{ex})}}(x_\alpha)\right]^2 \tag{7}$$

for each bin $\alpha = 0, 1, \ldots, P-1$ *in the histogram. The empirical potential for each experiment is*

$$U_m^{(\mathrm{ex})}(x_\alpha) = -k_B T \ln \rho_m^{(\mathrm{ex})}(x_\alpha), \tag{8}$$

from which we can obtain the mean values $\overline{U^{(\mathrm{ex})}}(x_\alpha)$ *and their errors* $\Delta_\alpha^{(\mathrm{U})}$ *in a similar way as in Eq.* (7)*. Assuming the potential to be harmonic, we have that*

$$\rho(x) = \sqrt{\frac{\kappa_x}{2\pi k_\mathrm{B} T}}\exp\left\{-\frac{\kappa_x}{2k_\mathrm{B}T}(x - x_{eq})^2\right\}. \tag{9}$$

Using this expression and the experimental dataset $\{x_\alpha, \overline{\rho^{(\mathrm{ex})}}(x_\alpha), \Delta_\alpha^{(\rho)}\}$*, we can find the estimates of the parameters* κ_x *and* x_eq *by means of the weighted non-linear least-square regression. Alternatively, we can use the experimental dataset* $\{x_\alpha, \overline{U^{(\mathrm{ex})}}(x_\alpha), \Delta_\alpha^{(\mathrm{U})}\}$ *allowing us to build a linear model and solve it analytically with linear least-square fitting (see Sec. 1.13 for more details on these concepts).*
As an example, Fig. 1 illustrates the empirical distributions and corresponding energy potentials of an optical tweezers with three different stiffness, corresponding to experiments I, II and III according to the

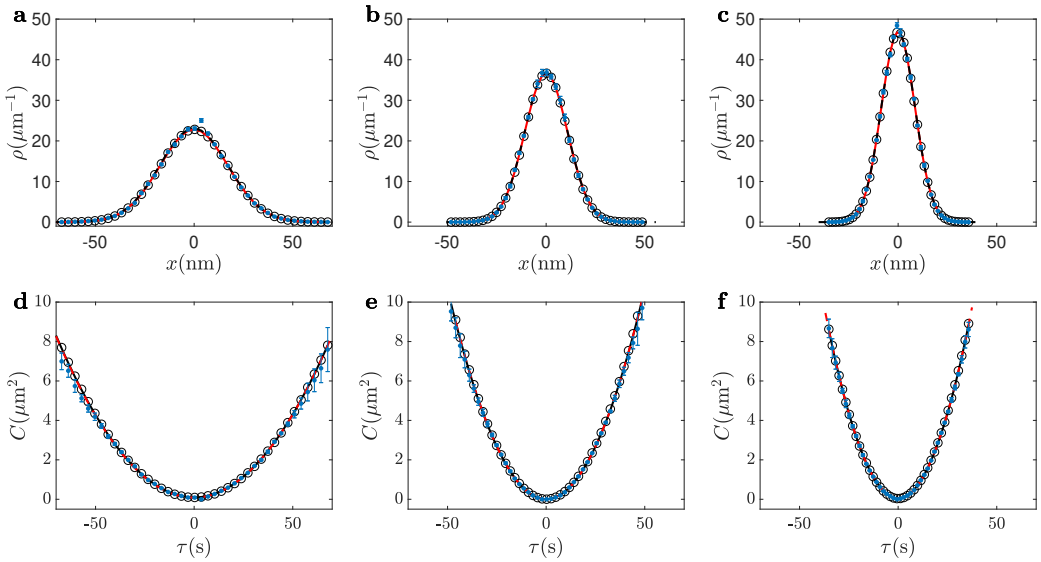

Fig. 1. Potential analysis. (a-c) Empirical distribution (dots) of the position of a particle in an optical tweezers with three different powers: 2.3 mW, 6.0 mW, and 9.2 mW (see Table 2 for more details of the experiment). The higher is the power, narrower is the distribution. (d-f) Corresponding potentials (data points) obtained by means of Eq. (8). Assuming an harmonic potential, the data points were fitted (solid lines) with both non-linear least square fitting, using directly the data points in the histogram, or with the analytical linear fitting, using the potential dataset. The resulting estimates of the trap stiffness using non-linear fitting are: $\kappa_x^{(\mathrm{ex})} = 13.9 \pm 0.2$ pN μm^{-1}, $\kappa_x^{(\mathrm{ex})} = 35.3 \pm 0.2$ pN μm^{-1}, and $\kappa_x^{(\mathrm{ex})} = 57.3 \pm 0.4$ pN μm^{-1}. For comparison, the resulting estimates obtained by means of the linear fitting can be found in Table 4.Laura and Alessandro. Make figure 2 rows and 3 columns. Get data from Alejandro and Isaac. + Prepare Python notebook to illustrate this fitting

data shown in Table 2, using $P = 50$ bins and the $M = 5$ experiments to estimate error bars for each bin. By means of either the distribution or the potential definitions, we are able to estimate the value of $\kappa_x^{(\mathrm{ex})}$ for the three experiments. The corresponding fitted curves for the three experiments are shown in solid lines in the distributions and in the potentials in Fig. (1)*. The estimates of $\kappa_x^{(\mathrm{ex})}$ using both approaches can be found in Table 4.*

To summarize, the potential method is fairly easy to implement and works for any conservative force with a potential that enables equilibrium of the particle in an accessible time. For a harmonic potential, the stiffness κ_x can be obtained directly by fitting the non-linear model of the distribution or by means of the linear regression with the potential. The non-linear fitting requires to use some numerical iterative method, making it more inefficient when compared to the linear fitting, for which an analytical solution can be given for the estimates. Finally, another limitation of this method is that in order to sample rare events, that is, in order to sample the anharmonicity of the potential for instance, one requires a number of measurements $N \sim \frac{1}{\rho(x)}$, and depending on the point x, N can be extraordinarily large.

1.3. Equipartition method

The equipartition method is a particular case of the potential method in which we assume a harmonic potential:

$$U(x) = \frac{\kappa_x}{2}(x - x_{eq})^2, \tag{10}$$

where κ_x is the trap stiffness and x_{eq} is the equilibrium position. Thus, the particle position distribution corresponds to the Gaussian distribution

$$\rho(x) = \sqrt{\frac{\kappa_x}{2\pi k_{\mathrm{B}}T}}\exp\left\{-\frac{\kappa_x}{2k_{\mathrm{B}}T}(x - x_{eq})^2\right\}. \tag{11}$$

From this, we find the thermal average of the potential

$$\langle U(x)\rangle = \frac{1}{2}\kappa_x\langle(x - x_{eq})^2\rangle = \frac{\kappa_x}{2}\int_{-\infty}^{\infty}\rho(x)(x - x_{eq})^2 dx = \frac{1}{2}k_{\mathrm{B}}T, \tag{12}$$

which is nothing more than the equipartition theorem, imposing that the energy associated with the potential harmonic degree of freedom is equal to $\frac{1}{2}k_{\mathrm{B}}T$. This provides a direct method to estimate κ_x by

$$\kappa_x = \frac{k_{\mathrm{B}}T}{\langle(x - x_{eq})^2\rangle}, \tag{13}$$

where we can estimate the equilibrium average $\langle(x - x_{eq})^2\rangle$ by a time average. As we have discussed in the previous analysis on the potential method, our time series may be correlated. Hence, instead of using the full time trace, we work with the uncorrelated subsample $\{\hat{x}_\ell^{(m)}\}_{\ell=1}^{L}$. For each $m = 1, \ldots, M$, an estimate of the ensemble average $\langle(x - x_{eq})^2\rangle$ is given by its sample variance

$$\sigma_{x,m}^{(\mathrm{ex})2} = \frac{1}{L}\sum_{\ell=1}^{L}\left(\hat{x}_\ell^{(m)} - x_{eq}^{(\mathrm{ex})}\right)^2, \quad x_{eq,m}^{(\mathrm{ex})} = \frac{1}{L}\sum_{\ell=1}^{L}\hat{x}_\ell^{(m)}, \tag{14}$$

where $x_{eq,m}^{(\mathrm{ex})}$ corresponds to the sample mean of the m-th experiment. Thus, for each experiment we obtain

$$\kappa_{x,m}^{(\mathrm{ex})} = \frac{k_{\mathrm{B}}T}{\sigma_{x,m}^{(\mathrm{ex})2}}. \tag{15}$$

Using the results of the M experiments, we calculate its mean value and variance, viz.

$$\kappa_x^{(\mathrm{ex})} = \frac{1}{M}\sum_{m=1}^{M}\kappa_{x,m}^{(\mathrm{ex})}, \quad \sigma_{(\kappa_x)}^2 = \frac{1}{M-1}\sum_{m=1}^{M}\left(\kappa_{x,m}^{(\mathrm{ex})} - \kappa_x^{(\mathrm{ex})}\right)^2, \tag{16}$$

respectively.

Applying these concepts to the dataset of the experiments I, II and III described in Table 2, yields: $\kappa_x^{(\mathrm{ex})} = 13.9 \pm 0.4\ pN\ \mu m^{-1}$, $\kappa_x^{(\mathrm{ex})} = 35.7 \pm 0.7\ pN\ \mu m^{-1}$, *and* $\kappa_x^{(\mathrm{ex})} = 57.6 \pm 1.2\ pN\ \mu m^{-1}$, *respectively. These estimates are consistent with the ones found in the potential method albeit with bigger errors. Since the estimation of* κ_x *goes as the inverse of the position squared, the effect of any random error in the position detection will always underestimate the value of the stiffness*[1]. *A dataset of position with an error* δ_x *would yield a variance* $\sigma_x^{(\mathrm{ex})2} = \sigma_x^2 + \delta_x^2$ *with* σ_x^2 *the exact value. This makes clear that having access to the uncertainty of position enable us to improve the measurement of the stiffness as follows:*

$$\kappa_{x,m}^{(\mathrm{ex})} = \frac{k_B T}{\sigma_{x,m}^{(\mathrm{ex})2} - \delta_x^2}. \tag{17}$$

Reconsidering the dataset of the experiments I, II and III described in Table 2, and assuming a typical error in the position of $\delta_x = 1$ nm, *yields:* $\kappa_x^{(\mathrm{ex})} = 13.9 \pm 0.4\ pN\ \mu m^{-1}$, $36.1 \pm 0.7\ pN\ \mu m^{-1}$ *and* $58.4 \pm 1.2\ pN\ \mu m^{-1}$. *This shows that the major contribution of* δ_x *is to the mean values, particularly for stronger traps, compared to the previous results.*

Since the equipartition analysis assumes we are in thermal equilibrium, the main disadvantage of this method is to be sure that $T_s \gg \Delta t \gg \tau_{\mathrm{ot},x}$, *so that the time series must be, in principle uncorrelated. However, as we will see from the method of the autocorrelation function, the equal time autocorrelation function corresponds to the equipartition result, and therefore, using the correlated time series is equally valid. Another aspect is that the errors in the position detection give rise to an underestimate of the stiffness. Other than this, equipartition is simpler, easy to implement and does not require fitting a function as it is the case for the potential method. Finally, it is worth pointing out that this method, like the previous one, is an equilibrium method and, therefore, it does not rely on the knowledge of the viscosity and the radius of the particle to obtain an estimate for the trap stiffness.*

1.4. Mean squared displacement (MSD) analysis

This is the first method that takes advantage of the time-correlated properties of the Brownian particle in a harmonic potential. From the Langevin equation (3) *with linear restoring force* $F(x) = -\kappa_x x$, *one can*

[1] On the other hand, if the data position is retrieved after a band pass filter operation, the variance will diminish and hence the stiffness is overestimated

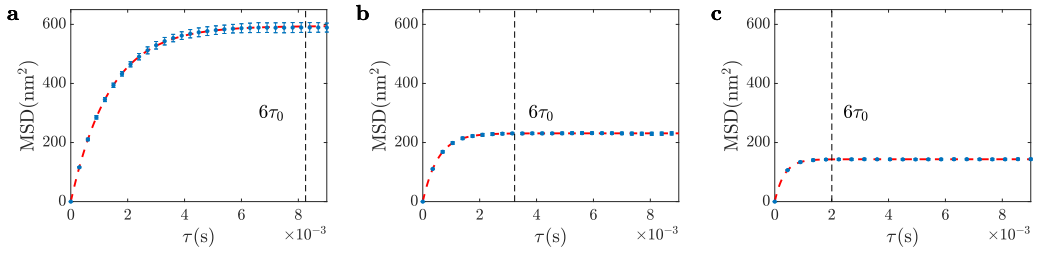

Fig. 2. MSD analysis. (a-c) Experimental MSD (dots) with its associated error and its corresponding fitting (solid lines) for the experiments I, II and III used throughout this section (see the details in Table 2). The data were fitted in the interval $[0.5\tau_{\mathrm{ot,x}}, 6\tau_{\mathrm{ot,x}}]$: the upper limit is shown with a dashed vertical line for each experiment. The resulting fitting values of the stiffness are: $\kappa_x^{(\mathrm{ex})} = 13.61 \pm 0.04\,\mathrm{pN}\,\mu\mathrm{m}^{-1}$, $\kappa_x^{(\mathrm{ex})} = 34.95 \pm 0.09\,\mathrm{pN}\,\mu\mathrm{m}^{-1}$, and $\kappa_x^{(\mathrm{ex})} = 56.40 \pm 0.16\,\mathrm{pN}\,\mu\mathrm{m}^{-1}$, and the relaxation times are: $\tau_{\mathrm{ot},x}^{(\mathrm{ex})} = 13.761 \pm 0.006 \times 10^{-4}$ s, $5.387 \pm 0.003 \times 10^{-4}$ s, $3.339 \pm 0.005 \times 10^{-4}$ s. As higher is the power shorter is the relaxation time $\tau_{\mathrm{ot,x}}$ and lower is the maximum value of the MSD. For comparison with other methods, the stiffness and the friction coefficient obtained by this method can be found in Table 3. Laura & Alessandro. Make figure 1 row and 3 columns. Get data from Alejandro & Isaac (it should be the same as for the previous figure). + Prepare Python notebook to illustrate these fittings.

show that the temporal mean squared displacement (MSD) of the Brownian particle is:

$$MSD_x(\tau) = \langle [x(t+\tau) - x(t)]^2 \rangle = \frac{2k_BT}{\kappa_x}\left[1 - e^{-\frac{|\tau|}{\tau_{\mathrm{ot},x}}}\right], \tag{18}$$

where $\langle(\cdots)\rangle$ denotes time average inherent of the stochastic process, and $\tau_{\mathrm{ot},x} = \frac{\gamma}{\kappa_x}$ is the characteristic relaxation time of the trap[2]*. Notice that $MSD_x(\tau)$ comprises two different time regimes: for $\tau \ll \tau_{\mathrm{ot},x}$, $MSD_x(\tau) \approx \frac{2k_BT}{\gamma}|\tau|$, the particle exhibits free diffusion, while for $\tau \gg \tau_{\mathrm{ot},x}$, $MSD_x(\tau) \approx \frac{2k_BT}{\kappa_x}$, the particle feels the harmonic potential and we recover the equipartition result given by equation* (13)*.*
If we are able to estimate $MSD_x(\tau)$ experimentally, we can obtain an estimate for the trap stiffness κ_x from a nonlinear fit to Eq. (18)*. To estimate MSD requires that the sampling time is shorter than the relaxation time, such that the time series $\{x_n^{(m)}\}_{n=1}^N$ is correlated for each $m = 1, \ldots, M$. If we denote $t_j = j\Delta t$ for $j = 1, \ldots, N$ and $\tau_\ell = \ell\Delta t$, the experimental estimate for the mean squared displacement is:*

$$MSD_{x,m}^{(\mathrm{ex})}(\tau_\ell) = \frac{1}{N-\ell}\sum_{j=1}^{N-\ell}[x_{j+\ell}^{(m)} - x_j^{(m)}]^2. \tag{21}$$

This gives a list of estimates $\{MSD_{x,m}^{(\mathrm{ex})}(\tau_\ell)\}_{m=1}^M$ for the MSD, from which to obtain its experimental mean and variance:

$$\begin{aligned}
\overline{MSD_x^{(\mathrm{ex})}(\tau_\ell)} &= \frac{1}{M}\sum_{m=1}^{M} MSD_{x,m}^{(\mathrm{ex})}(\tau_\ell), \\
\Delta_{\ell,\ell'}^{[MSD^{(\mathrm{ex})}]} &= \frac{1}{M-1}\sum_{m=1}^{M}\left(MSD_{x,m}^{(\mathrm{ex})}(\tau_\ell) - \overline{MSD_x^{(\mathrm{ex})}(\tau_\ell)}\right)\left(MSD_{x,m}^{(\mathrm{ex})}(\tau_{\ell'}) - \overline{MSD_x^{(\mathrm{ex})}(\tau_{\ell'})}\right).
\end{aligned} \tag{22}$$

Notice that, as in this case the experimental data is time-correlated, we need the covariance matrix when inferring the parameters from the non-linear fitting. With the experimental dataset $\{\overline{MSD_x^{(\mathrm{ex})}(\tau_\ell)}, \Delta_{\ell,\ell'}^{[MSD^{(\mathrm{ex})}]}\}$ together with the theoretical model of the MSD in Eq.(18)*, we can proceed to construct χ^2 according to Eq.* (71) *and minimize numerically to find the estimates κ_x and $\tau_{\mathrm{ot,x}}$.*
Before proceeding with the non-linear fitting, there are several aspects to consider: first of all, as the MSD show two distinct time-regimes, we must be sure to have a good balance of points in both regimes in order to avoid one respect to the other. This implies to determine a maximum time for τ_ℓ. Another aspect is that the experimental error of the MSD increases as the lag time grows since the number of data points used to estimate MSD diminishes. Finally, as he MSD goes as the position squared, we have to take care on the error of the position detection, particularly in the short time regime where the influence in the experimental points is relatively stronger and neglecting these errors may give rise to some outliers points, producing and overfitting of the short time regime. With this in mind, practically with the experimental MSD defined in the interval that goes from some fractions of $\tau_{\mathrm{ot},x}$ to some values of $\tau_{\mathrm{ot,x}}$ is enough to compute the fitting. If we have access to the errors of position, then the fitting interval may be extended, although this may not be necessary as we are only inferring two parameters.
For the data recorded during experiments I, II and III, it is sufficient to choose τ_ℓ to be inside the interval $[0.5\tau_{\mathrm{ot,x}}, 6\tau_{\mathrm{ot,x}}]$. After performing the non-linear fitting and estimating the errors using the method explained in [5], we obtain the following results for the trap stiffness for the three experiments: $\kappa_x^{(\mathrm{ex})} = 13.61 \pm 0.04\,\mathrm{pN}\,\mu\mathrm{m}^{-1}$, $\kappa_x^{(\mathrm{ex})} = 34.95 \pm 0.09\,\mathrm{pN}\,\mu\mathrm{m}^{-1}$, and $\kappa_x^{(\mathrm{ex})} = 56.40 \pm 0.16\,\mathrm{pN}\,\mu\mathrm{m}^{-1}$, respectively. Similarly, the estimates for the relaxation times for each experiment are:

[2]Following, for instance, [4], we first see that the formal solution of the Langevin equation (3) is given by

$$x(t) = x(0)e^{-t/\tau_{\mathrm{ot},x}} + \sqrt{2D}\int_0^t ds W_x(s)e^{-(t-s)/\tau_{\mathrm{ot},x}}. \tag{19}$$

From here one can find, using the properties of white noise of $W_x(s)$, that

$$\overline{x(t_1)x(t_2)} = x^2(0)e^{-(t_1+t_2)/\tau_{\mathrm{ot},x}} + D\tau_{\mathrm{ot},x}\left(e^{-|t_1-t_2|/\tau_{\mathrm{ot},x}} - e^{-(t_1+t_2)/\tau_{\mathrm{ot},x}}\right). \tag{20}$$

This result can be used to derive the expression for the $\mathrm{MSD}_x(\tau)$ given by equation (18).

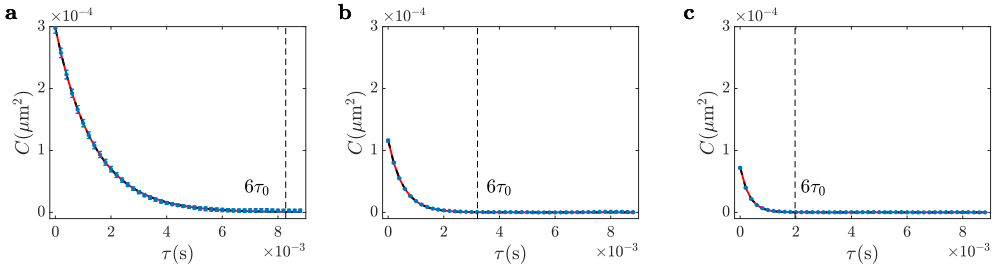

Fig. 3. ACF analysis. (a-c) Autocorrelation function for the experiments I, II and III (see Table 2 for the details of the parameters). Solid curves show the resulting fitting using directly the ACF function and applying a non-linear procedure. The resulting fitting values of the stiffness are: $\kappa_x = 13.91 \pm 0.01$ pN μm^{-1}, $\kappa_x^{(\text{ex})} = 35.60 \pm 0.04$ pN μm^{-1}, and $\kappa_x^{(\text{ex})} = 56.91 \pm 0.07$ pN μm^{-1}. As higher is the power, faster the ACF function falls and higher are the values of the stiffness. Laura & Alessandro. Make figure 1 row and 3 columns. Get data from Alejandro & Isaac (it should be the same as for the previous figure). + Prepare Python notebook to illustrate these fittings.

$\tau_{\text{ot},x}^{(\text{ex})} = (13.761 \pm 0.006) \times 10^{-4}$ s, $\tau_{\text{ot},x}^{(\text{ex})} = (15.387 \pm 0.003) \times 10^{-4}$ s, *and* $\tau_{\text{ot},x}^{(\text{ex})} = (13.339 \pm 0.005) \times 10^{-4}$ s. *Finally, we can combined these two sets of results to estimate the friction coefficient, by using the formula* $\gamma = \kappa_x \tau_{\text{ot},x}$. *This results into* $\gamma^{(\text{ex})} = 19.17 \pm 0.01$ pN ms μm^{-1}, $\gamma^{(\text{ex})} = 19.30 \pm 0.01$ pN ms μm^{-1}, *and* $\gamma^{(\text{ex})} = 19.30 \pm 0.03$ pN ms μm^{-1}, *respectively. All these results are summarised in Figs. 2(a-c) and reported in Table 4.*

The MSD analysis has a few clear advantages: first of all, we can use all the information of each time series to obtain a series of estimates $MSD_{x,m}^{(\text{ex})}(\tau_\ell)$, *which implies, in turn, that errors of the estimates for the trap stiffness tend to be smaller than the previous methods. Secondly, since this analysis takes advantage of the relaxation properties of the problem we are able to infer not only equilibrium quantities, like the trap stiffness, but also the friction coefficient, which is not directly accessible with the previous equilibrium methods. Unfortunately, the MSD analysis relies on fitting a function with correlated errors, and being careful to have a good balance of data points between the free diffusion regime and the equipartition one.*

1.5. Autocorrelation function (ACF)

Starting from the Langevin equation (3)*, the position autocorrelation function (ACF) is [4]*

$$C_x(\tau) = \langle x(t+\tau)x(t)\rangle = \frac{k_\text{B}T}{\kappa_x} e^{-\frac{|\tau|}{\tau_{\text{ot},x}}} . \tag{23}$$

From a correlated time series sampled at regular time steps Δt*, we can estimate the ACF by using*

$$C_{x,m}^{(\text{ex})}(\tau_\ell) = \frac{1}{N-\ell} \sum_{j=1}^{N-\ell} x_{j+\ell}^{(m)} x_j^{(m)}, \tag{24}$$

which gives a set of estimates $\{C_{x,m}^{(\text{ex})}(\tau_\ell)\}_{m=1}^M$ *for each experiment* $m = 1, \ldots, M$*. From these estimates, we obtain its empirical mean and covariance matrix as*

$$\begin{aligned} \overline{C_x^{(\text{ex})}(\tau_\ell)} &= \frac{1}{M} \sum_{m=1}^{M} C_{x,m}^{(\text{ex})}(\tau_\ell), \\ \Delta_{\ell,\ell'}^{[C_x^{(\text{ex})}]} &= \frac{1}{M-1} \sum_{m=1}^{M} \left(C_{x,m}^{(\text{ex})}(\tau_\ell) - \overline{C_x^{(\text{ex})}(\tau_\ell)} \right) \left(C_{x,m}^{(\text{ex})}(\tau_{\ell'}) - \overline{C_x^{(\text{ex})}(\tau_{\ell'})} \right) . \end{aligned} \tag{25}$$

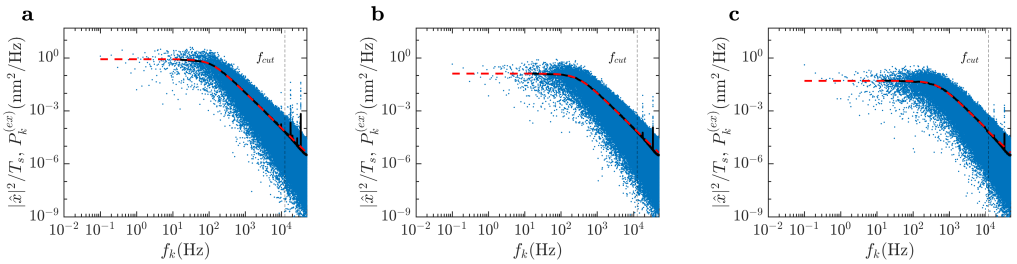

Fig. 4. Power spectral density analysis. (a-c) By means of equation (34) we compute $|\hat{x}|^2/T_s$, shown in blue, then this is compressed by windowing, with $Nw = 2000$, to obtain the experimental power spectral density, $P_k^{(\mathrm{ex})} = \langle |\hat{x}|^2/T_s \rangle_{n_w}$, shown in circle dots, both represented in loglog scale. The Lorentzian defined by equation (26) is fitted to $P_k^{(\mathrm{ex})}$ according to Eqs.(30) and (31). The resulting Lorentzian is plotted with solid lines. The vertical dotted line indicates the maximum frequency used to perform the fitting and avoid aliasing; in this example $\max\{f_k\} = f_{\mathrm{Nyq}}/4 = f_s/8$. (d-f) Result of the fitting for three series of data used in this manuscript (see Table 4 for the resulting estimates and Table 1 for the details of the experiments). Laura & Alessandro. Make figure 1 row and 3 columns. Get data from Alejandro & Isaac (it should be the same as for the previous figure). + Prepare Python notebook to illustrate these fittings.

In this case we can directly estimate the stiffness κ_x and the relaxation time $\tau_{\mathrm{ot},x}$, and hence the friction coefficient $\gamma = \tau_{\mathrm{ot},x}\kappa_x$. Using the the autocorrelation equation (23)*, we can build $\chi^2(\kappa_x, \tau_{\mathrm{ot},x})$ according to equation* (71) *and minimize with respect to the parameters, solving the resulting set of equations by means of non-linear procedures using iterative solutions. Another possibility is to use the logarithm of the autocorrelation instead, $\ln C_x(\tau) = \ln k_B T/\kappa_x - \tau/\tau_{\mathrm{ot},x}$ and perform a linear regression. In this case, the experimental dataset is $\{\overline{\ln C_x^{(\mathrm{ex})}(\tau_\ell)}\}$ together with their covariance matrix for the M experiments.*

Figure 3 shows the resulting mean $\overline{C_x^{(\mathrm{ex})}(\tau_\ell)}$ with error bars, together with the resulting fitting for each set of data, of the experiments used as examples in this section (see Table 2 for more details). Similar to the MSD method, the ACF allow us to estimate the friction coefficient γ beside the stiffness. Since the ACF function decays exponentially with time, only the values corresponding to short times, around the relaxation time, are relevant to get the information of the confining potential. In the same way as the MSD, this method requires sampling times much lower than the characteristic time of the trap, $\Delta t \ll \tau_{\mathrm{ot},x}$, at the same time that the total time has to be very large, $T_s \gg \tau_{\mathrm{ot},x}$, in order to have a good estimation of the ACF. In this way, the fitting can be performed only with data corresponding up to some values of $\tau_{\mathrm{ot},x}$. The estimated values of κ_x using non-linear fitting are reported in the caption of Fig. 3, and for comparison all the estimates of κ_x, including the ones using linear-regression, and the friction coefficients are reported in Table 4. We can see from these results, that the estimates obtained from the MSD ad the ACF method are comparable, both using non-linear and analytical linear regression, nevertheless the main difference is the time that the computer algorithm take to process the information, while the ACF can be implemented with efficient algorithms to compute the autocorrelation, based on the Fast Fourier transform, the MSD does not have any equivalent method so the crawling discrete operation defining the MSD is unavoidable.

Notice that in this case the error of the estimate $\kappa_x^{(\mathrm{ex})}$ is bigger than the one obtained from MSD. This is expected from the expression of the autocorrelation function given by equation (23)*, whose initial value is solely determined by the trap stiffness and not the decaying behavior. In other words: we only have one data point to estimate $\kappa_x^{(\mathrm{ex})}$. The estimates for the rest of the experiments can be found in Table 4.*

1.6. Power spectral density (PSD)

Calibration of an optical tweezer by means of the power spectral density (PSD) is considered to be one of the most reliable methods due to its ability to remove common sources of noise with relative ease since one

works in frequency space directly. As before, we first discuss the theoretical description and then its experimental estimate, from which, upon a fitting procedure, one can infer the optical properties of the trap. The treatment shown in this section is based on Ref. [6].

Starting from the Langevin equation (3) *with* $F(x) = -\kappa_x x$ *and performing the Fourier transform, one can obtain the typical Lorentzian form of PSD, defined as the expected value of the average energy in the frequency domain,*

$$P(f) = \langle |\widetilde{x}(f)|^2 \rangle = \frac{1}{2\pi^2} \frac{D}{f_{c,x}^2 + f^2}, \tag{26}$$

where $\widetilde{x}(f)$ *is*

$$\widetilde{x}(f) = \frac{1}{\sqrt{T}} \int_0^T x(t) e^{-i2\pi f t} dt,$$

and $f_{c,x} = \kappa_x / 2\pi\gamma = 1/2\pi\tau_{\mathrm{ot},x}$ *is the corner frequency. To derive equation* (26)*, we have used the fact that the spectrum of the zero-mean white noise,* $|\widetilde{W}_x(f)|^2$*, has an exponential distribution with an expected value* $\langle |\widetilde{W}_x(f)|^2 \rangle = 1$.

In practice, we have a sampled trajectory with a frequency $f_\mathrm{s} = 1/\Delta t$ *up to a time* T_s*, that is, we obtain a time series* $x_j = x(t_j)$*, with* $t_j = j\Delta t$ *and* $j = 1, \ldots, N$*, which is used to perform the discrete Fourier transform (DFT),*

$$\hat{x}_k = \Delta t \sum_{j=1}^{N} e^{i2\pi f_k t_j} x_j = \Delta t \sum_{j=1}^{N} e^{i2\pi jk/N} x_j. \tag{27}$$

It is expected that $\langle |\hat{x}_k|^2 \rangle / T_\mathrm{s} \approx \langle |\tilde{x}(f_k)|^2 \rangle$ *when* $f_\mathrm{s} \gg f_{c,x}$*, so it is important in this procedure to sample the trajectory at frequencies some orders of magnitude higher than the corner frequency in order to get the relevant information of the process. On the other hand, the discrete PSD will suffer from aliasing, which is inherited from the DFT operation owing to the unavoidable loss of information when sampling. A simple formula for the expected value of the aliased power spectrum can be derived from the discretized Einstein-Ornstein-Uhlembeck process [6], yielding*

$$P_k^{(\mathrm{aliased})} = \frac{\langle |\hat{x}_k| \rangle}{T_s} = \frac{(\Delta x)^2 \Delta t}{1 + c^2 - 2c\cos(2\pi f_k \Delta t / N)}, \tag{28}$$

where $\Delta x = ((1 - c^2) D / 2\pi f_{c,x})^{1/2}$ *and* $c = e^{-2\pi f_{c,x}/f_\mathrm{s}}$*. As long as we sample at frequencies some orders of magnitude higher than the corner frequency, we can mitigate the aliasing by simply cropping the spectrum at a frequency below the Nyquist (*$f_\mathrm{Nyq} = f_\mathrm{s}/2$*).*

The expected value in the PSD can be estimated by averaging the experimental values $|\hat{x}_k|^2 / T_\mathrm{s}$ *over a set of* M *experiments. In practice this is complicated since one would need to acquire hundreds of experiments to have a good estimation. Instead it is common to apply a compression process to obtain a good estimation of the expected value with only one or a few experiments. Windowing is the most common compression process, it divides the frequency domain in* N_w *narrow and equidistant subdomains with* n_w *values, whose average represents the expected value at the corresponding mean frequency of the subdomain. This gives rise to the reduced experimental dataset,* $P_k^{(\mathrm{ex})} = \langle |\hat{x}_k|^2 / T_\mathrm{s} \rangle_{n_\mathrm{w}}$ *with* $k = 0, 1, 2, ..., N_\mathrm{w} - 1$*. By this procedure, the error in the expected value is* $\sigma_k^{(\mathrm{ex})} = P_k^{(\mathrm{ex})} / \sqrt{n_\mathrm{w}}$*. When there are more than one realization of the experiment, it is also possible compress first the experiments and then average all of them, giving an error* $\sigma_k^{(\mathrm{ex})} = P_k^{(\mathrm{ex})} / \sqrt{M n_\mathrm{w}}$.

Once the experimental PSD is estimated, least square fitting are applied in order to estimate the unknown parameters ($f_{c,x}$ *and* D*). Using directly the model* (26) *and the data set* $\{f_k, P_k^{(\mathrm{ex})}\}$ *with their associated weights,* $W_k = 1/(\sigma_k^{(\mathrm{ex})})^2$*, we can build* $\chi^2(f_{c,x}, D)$ *according to the definition* (71) *and then apply the non-linear fitting procedure with a numerical solution for the estimates. As we have mention before, this procedure arises the risk to obtain wrong results if the starting points and the converging conditions are not properly defined. On the other hand, an analytical linear fitting, can be applied if we use the experimental dataset* $\{f_k^2, 1/P_k^{(\mathrm{ex})}\}$ *instead, with weights given by* $W_k = 1/(P_k^{(\mathrm{ex})-1} / \sqrt{n_\mathrm{w}})^2$ *and the linear model*

$1/P(f) = 2\pi^2 f^2/D + 2\pi^2 f_{c,x}^2/D$. *An alternative analytical solution can be found by minimizing*

$$\chi^2(f_{c,x}^2, D) = \frac{1}{N_\mathrm{w}} \sum_k^{N_\mathrm{w}} \left(\frac{P_k^{(\mathrm{ex})} - P(f_k; f_{c,x}^2, D)}{P(f_k; f_{c,x}^2, D)/\sqrt{n_\mathrm{w}}} \right)^2 . \tag{29}$$

according to Ref. [6], giving an analytical solution as well[3].
As an example, Figs. 4(a-c) show the values $|\hat{x}_k|^2/T_\mathrm{s}$ *of a sampled trajectory of a particle in an optical tweezer (Experiments I II and III in Tables 2 and 4) computed by means of the fast Fourier transform:*

$$\frac{|\hat{x}_k|^2}{T_\mathrm{s}} = \frac{\Delta t^2}{T_\mathrm{s}} |\mathrm{FFT}\{\{x_j\}_{j=1}^N\}_k|^2 \quad with \quad f_k = \frac{k}{T_\mathrm{s}} \quad for\ k = 0, 1, 2, ..., N/2. \tag{34}$$

Their expected values are obtained by means of compression, using $N_\mathrm{w} = 2000$ *windows, shown in circle dots in Fig. 4. Once the PSD is obtained, these data are used to fit the Lorentzian function given by equation* (26) *according to Eqs.* (30) *and* (31)*. To avoid the aliasing effect, giving rise to the plateau at the end of the the data points, the fitting was not performed with the whole data set, but only with the data corresponding to frequencies lower than* $f_{max} = f_\mathrm{Nyq}/4 = f_\mathrm{s}/8$*. Repeating this procedure for* $M = 5$ *experiments, one obtains the mean values of the estimates:* $\kappa_x^{(\mathrm{ex})} = 2\pi\gamma f_{c,x}^{(\mathrm{ex})} = 13.7 \pm 0.2\,\mathrm{pN}\,\mu\mathrm{m}^{-1}$ *and* $D_x^{(\mathrm{ex})} = 0.2105 \pm 0.0006\,\mu\mathrm{m}^2\,\mathrm{s}^{-1}$ *and* $\gamma^{(\mathrm{ex})} = D_x^{(\mathrm{ex})}/(k_\mathrm{B}T) = 19.68 \pm 0.05\,\mathrm{pN\,ms}\,\mu\mathrm{m}^{-1}$*. Figure 4(b) show the experimental PSD and fitting of the three experiments corresponding to three different powers (experiments I-III in Table 2) in the optical tweezers (see Table 4 for the resulting estimates).*
In contrast to other methods, the PSD analysis is very robust to unwanted periodic noise in the extracted trajectory of the particle, due to, for example, illumination, electronic noise, fan noise of different electronic components inside the laboratory or even some resonant vibration that is difficult to isolate with optical tables. In Fig. 4 we can see one narrow peak of the experimental PSD around 94 Hz*, which is practically ignored during the fitting procedure given that is only represented by one or two points.*

[3] The analytical solutions for the estimates using χ^2 defined by Eq. (29) is

$$f_{c,x}^{(\mathrm{ex})} = \sqrt{\frac{S_{0,1}S_{2,2} - S_{1,1}S_{1,2}}{S_{1,1}S_{0,2} - S_{0,1}S_{1,2}}}, \tag{30}$$

$$D^{(\mathrm{ex})} = 2\pi^2 \left(\frac{S_{0,2}S_{2,2} - S_{1,1}^2}{S_{1,1}S_{0,2} - S_{0,1}S_{1,2}} \right), \tag{31}$$

where

$$S_{p,q} = \sum_k^{N_\mathrm{w}} f_k^{2p} P_k^{(\mathrm{ex})\,\mathrm{q}}.$$

The error for the estimates are

$$\frac{\sigma(f_{c,x}^{(\mathrm{ex})})}{f_{c,x}^{(\mathrm{ex})}} = \frac{1}{\sqrt{(u-v) f_{c,x}^{(\mathrm{ex})} T_\mathrm{s}}}, \tag{32}$$

$$\frac{\sigma(D^{(\mathrm{ex})})}{D^{(\mathrm{ex})}} = \sqrt{\frac{u}{(x_\mathrm{max} - x_\mathrm{min})\pi f_{c,x}^{(\mathrm{ex})} T_\mathrm{s}}}, \tag{33}$$

where $x_\mathrm{min} = f_\mathrm{min}/f_{c,x}^{(\mathrm{ex})}$ and $x_\mathrm{max} = f_\mathrm{max}/f_{c,x}^{(\mathrm{ex})}$,

$$u = \frac{2x_\mathrm{max}}{1 + x_\mathrm{max}^2} - \frac{2x_\mathrm{min}}{1 + x_\mathrm{min}^2} + 2\arctan\left(\frac{x_\mathrm{max} - x_\mathrm{min}}{1 + x_\mathrm{max}x_\mathrm{min}} \right),$$

$$v = \frac{4}{x_\mathrm{max} - x_\mathrm{min}} \arctan^2\left(\frac{x_\mathrm{max} - x_\mathrm{min}}{1 + x_\mathrm{max}x_\mathrm{min}} \right).$$

1.7. Drift method

The drift method [7–9] relies on the fact that, on average the drag force must be equal to the optical force. From Langevin's equation (3)*, this implies that*

$$F(x_0) = 6\pi\eta a \frac{\langle \Delta x \rangle_{x_0}}{\Delta t}\,, \tag{35}$$

where $\langle \Delta x \rangle_{x_0}$ *is usually referred to the local drift and corresponds to the average displacement of the particle in a interval* Δt *starting at a point* x_0 *and moves under the external force* F_{x_0}*. Now, to estimate from experimental data the particle's average local drift one proceeds as follows: each time* t *the particle selects a given volume element near* x_0*, the local drift associate to this volume is estimated as*

$$\langle \Delta x \rangle_{x_0} = \frac{1}{S}\sum_{i=1}^{S} \left[x_i(t+\Delta t) - x_i(t) \right]\,, \tag{36}$$

where S *corresponds to the number of visits to that particular volume within the recorded time series. Notice that this method has a series of disadvantages. First of all, the size of the volume element near* r_0 *must be small enough to probe correctly the spatial variations of the force field. On the other side, the position of the particle must be measure with a precision much smaller than that of the volume element. Although equation* (35) *is valid in most applications where the diffusion coefficient is constant, there may be more complex scenarios in which the diffusion coefficient can be space-dependent leading to a "spurious drift". This space-dependency is mostly due to the interactions between close particles or between a particle and a close surface. The effects of spurious drift has to be taken into account whenever we estimate forces from induced drift measurements. Importantly, neglecting this correcting factors from the spurious drift may lead to the wrong amplitude and sign of the forces acting on micro-objects suspended in liquids, such as colloidal suspensions [9, 10]. When diffusion coefficient is spatially-dependent a diffusion gradient term can be added to equation* (35) *leading to*

$$F(x_0) = \gamma(x_0)\frac{\langle \Delta x \rangle_{x_0}}{\Delta t} - \alpha\gamma(x_0)\frac{dD(x_0)}{dx_0}\,. \tag{37}$$

Equation (37) *is usually referred to as "spurious force". Here,* α *may take values in the interval* $[0, 1]$*, depending on the specific stochastic process being modelled. In particular,* $\alpha = 1$ *corresponds to a colloidal particle in a thermal bath [11]. Finally, whenever the diffusion coefficient is position-dependent, it leads naturally to multiplicative noise, which is the product of a state-dependent prefactor proportional to the square root of the diffusion coefficient and a state-independent Gaussian white noise function [11]. There are two different convections for dealing with multiplicative noise: the Ito convection, where the state-dependent prefactor is evaluated before the Gaussian noise [12], and the Stratonovich convention, where the* δ*-correlated white noise is obtained as a limit of a noise with a nonzero correlation time [13].*

1.8. Force reconstruction via maximum-likelihood-estimator analysis (FORMA)

The force reconstruction via maximum-likelihood-estimator analysis (FORMA) was introduced recently to retrieve the force field acting on a Brownian particle from the analysis of its displacements [14]. This method is able to estimate accurately the conservative and non-conservative components of the force field with important advantages over the previously discussed techniques, being parameter-free, requiring ten-fold less data and executing orders-of-magnitude faster.
The idea is fairly simple. For simplicity let us consider again the case of the harmonic potential, and suppose that after a time interval $\Delta t \ll \tau_{\mathrm{ot},x}$ *the Brownian particle is at a position* x*, having started at position* x_0*. Repeating this pair of measurements* N *times, we construct the likelihood of observing this set of measurements, viz*

$$\mathcal{L}(\{x_n\}_{n=1}^N | \{x_{0n}\}_{n=1}^N, \kappa_x/\gamma, D) = \frac{1}{(4\pi D\Delta t)^{N/2}} \exp\left[-\frac{1}{4D}\sum_{n=1}^{N} \Delta t \left(\frac{x_n - x_{0n}}{\Delta t} + x_{0n}\frac{\kappa_x}{\gamma} \right)^2 \right]. \tag{38}$$

Fig. 5. FORMA. Laura & Alessandro. Add figure for FORMA.

By maximizing the log-likelihood with respect to the diffusion constant D and the trap stiffness κ_x one obtains the following maximum likelihood estimators (MLEs) for a given time series $\{x_\ell^{(m)}\}_{\ell=1}^N$:

$$\frac{\kappa_{x,m}^{(\mathrm{ex})}}{\gamma} = -\frac{\sum_{n=1}^{N-1} x_n^{(m)} \frac{x_{n+1}^{(m)} - x_n^{(m)}}{\Delta t}}{\sum_{n=1}^{N-1} [x_n^{(m)}]^2}, \qquad D_m^{(\mathrm{ex})} = \frac{\Delta t}{2N} \sum_{n=1}^{N-1} \left(\frac{x_{n+1}^{(m)} - x_n^{(m)}}{\Delta t} + \frac{\kappa_{x,m}^{(\mathrm{ex})}}{\gamma} x_n^{(m)} \right)^2 . \tag{39}$$

From these equations, the idea is to first estimate the ratio $\frac{\kappa_{x,m}^{(\mathrm{ex})}}{\gamma}$, and use it the estimate of the diffusion constant $D_m^{(\mathrm{ex})}$. Once we have the latter, we can use the fluctuation-dissipation theorem, $D = k_B T/\gamma$, to estimate the friction coefficient and, finally κ_x. The standard errors for these estimates are obtained from the mean and standard deviations from repeated experiments, as done in [14]. Being more precise, we use the $m = 1, \ldots, M$ time series to obtain the list of estimates $\{\kappa_{x,m}^{(\mathrm{ex})}\}_{m=1}^M$ and $\{D_m^{(\mathrm{ex})}\}_{m=1}^M$, to yield the empirical mean and variances:

$$\begin{aligned} \overline{\kappa_x^{(\mathrm{ex})}} &= \frac{1}{M} \sum_{m=1}^{M} \kappa_{x,m}^{(\mathrm{ex})}, \qquad \Delta^{(\kappa_x)} = \frac{1}{M-1} \sum_{m=1}^{N_{exp}} \left(\kappa_{x,m}^{(\mathrm{ex})} - \overline{\kappa_x^{(\mathrm{ex})}} \right)^2, \\ \overline{D^{(\mathrm{ex})}} &= \frac{1}{M} \sum_{m=1}^{N_{exp}} D_m^{(\mathrm{ex})}, \qquad \Delta^{(D)} = \frac{1}{M-1} \sum_{m=1}^{M} \left(D_m^{(\mathrm{ex})} - \overline{D^{(\mathrm{ex})}} \right)^2 . \end{aligned} \tag{40}$$

FORMA provides an alternative way to get error estimates without having to repeat the experiment. Indeed, if we perform a Taylor expansion of the log-likelihood around the MLEs up to second order, we obtain a Gaussian approximation for $\mathcal{L}(\{x_n\}_{n=1}^N | \{x_{0n}\}_{n=1}^N)$. This yields the following standard deviations for $\kappa_x^{(\mathrm{ex})}$ and $D^{(\mathrm{ex})}$

$$\sigma_{D^{(\mathrm{ex})}} = D^{(\mathrm{ex})} \sqrt{\frac{2}{N}}, \qquad \sigma_{\kappa_x^{(\mathrm{ex})}} = \sqrt{\frac{2D^{(\mathrm{ex})}}{\Delta t \sum_{n=1}^N x_{0n}^2}} . \tag{41}$$

Let us apply FORMA for the experiment I, II and III detailed in Table 2. Here we will use the two different methods to retrieve the error estimates and check if they are indeed comparable. We first follow the route as in [14] and use the data from the 5 experiments to obtain mean values and error bars. From formulas (39) and (40), we obtain $\kappa_x^{(\mathrm{ex})} = 14.0 \pm 0.4\,\mathrm{pN}\,\mu\mathrm{m}^{-1}$, $\kappa_x^{(\mathrm{ex})} = 35.9 \pm 0.7\,\mathrm{pN}\,\mu\mathrm{m}^{-1}$, and $\kappa_x^{(\mathrm{ex})} = 58.1 \pm 1.1\,\mathrm{pN}\,\mu\mathrm{m}^{-1}$, respectively. Next let us consider the second approach, consisting in taking a single time series, let us say the one corresponding the first experiment, and then estimate the errors using equations (41). This yields: $\kappa_x^{(\mathrm{ex})} = 13.9 \pm 0.3\,\mathrm{pN}\,\mu\mathrm{m}^{-1}$, $\kappa_x^{(\mathrm{ex})} = 35.9 \pm 0.5\,\mathrm{pN}\,\mu\mathrm{m}^{-1}$, and $\kappa_x^{(\mathrm{ex})} = 58.1 \pm 0.6\,\mathrm{pN}\,\mu\mathrm{m}^{-1}$, for experiments I, II, and III, respectively. These results are obviously compatible with the first approach. This remark is important, as it allows us to gather all the time series together, as if they were a single experiment to get a better estimates with smaller errors. Finally, using the fluctuation-dissipation theorem we obtain the following estimates for the friction: $\gamma^{(\mathrm{ex})} = 21.2 \pm 0.3\,\mathrm{pN\,ms}\,\mu\mathrm{m}^{-1}$, $\gamma^{(\mathrm{ex})} = 23.7 \pm 0.3\,\mathrm{pN\,ms}\,\mu\mathrm{m}^{-1}$, and $\gamma^{(\mathrm{ex})} = 26.3 \pm 0.5\,\mathrm{pN\,ms}\,\mu\mathrm{m}^{-1}$, respectively. Final estimates for the rest of experiments can be found in Table 4. Comparing these results with the ones obtained by the other methods, we can see big discrepancies in the diffusion and hence in the friction coefficient, comparing also with theoretical values ($D^{(\mathrm{th})}$ and $\gamma^{(\mathrm{th})}$ in Table 2). I am including the values of gamma obtained with a subsampling of 10, otherwise it gives a biger discrepancy. The problem with this is that the number of of points are reduced to 1e5, introducing also an error which is more important for larger k's.

Since FORMA only depends on the local variables of the trajectory, that is the positions and their corresponding displacements, it allows to retrieve the forces of arbitrary optical landscapes, including non-conservative forces as we shall see later, and hence it does not need a trajectory with regular sampling, commonly required in the other methods. This is particularly useful when the problem is to retrieve the forces of extended potentials, where the particle beither reaches the equilibrium nor is able to explore the whole space by itself, as it was shown in Ref. [14] for a dual optical tweezer and an speckle pattern. On the other hand, the local property of FORMA makes it more sensitive to the resolution in the video-microscopy

system, which directly affects the estimate of the diffusion $D^{(\mathrm{ex})}$ and the friction coefficient $\gamma^{(\mathrm{ex})}$, as it is seen in previous examples. Subsampling the whole trajectory makes these effect less significant and better estimates can be obtained.
FORMA has a considerable number of advantages compared to the previous methods, as one can use the whole time series and it does not require any fitting neither is restricted to harmonic potentials. Moreover, slightly generalizing the work in [14] one does not need to divide the time series in various parts to estimate error bars, since maximum likelihood estimators naturally provide estimates for the errors. The only drawback is the need of accurate positions and small sampling times Δt. The last can be solved by generalizing the solution for any arbitrary time interval Δt, as introduced recently in Ref. [15].

1.9. Bayesian inference

The method FORMA uses ideas of non-Bayesian linear regression models [14] to infer the properties of the trap and the Brownian particle. Other methods have used Bayesian inference to infer optical forces [15–19], but these tend to use non-informative priors. Recently, we have derived a Bayesian approach using conjugate priors, which renders very simple formulas for the posterior distribution, for which all moments and marginal posteriors are known. Being more precise, suppose that the parameters we want to infer are the diffusion constant D and the ratio κ_x/γ. Let $P_0(\kappa_x/\gamma, D)$ be the a priori *probability distribution we have for those parameters. Then, by Bayes' rule, the posterior probability of these parameters given a time series is:*

$$P(\kappa_x/\gamma, D) = \frac{\mathcal{L}(\{x_n\}_{n=1}^N|\{x_{0n}\}_{n=1}^N, \kappa_x/\gamma, D)P_0(\kappa_x/\gamma, D)}{Z} \tag{42}$$

with Z being a normalization factor. Considering a conjugate prior $P_0(\kappa_x/\gamma, D)$ for the model's likelihood, we obtain the following marginal posterior distribution for the trap stiffness and the diffusion constant [20]

$$\begin{aligned} P_D(x) &= \mathrm{InvGamm}\,(x|\alpha_N, \beta_N)\,, \\ P_{\kappa_x/\gamma}(x) &= \frac{\Gamma\left(\frac{2\alpha_N+1}{2}\right)}{\Gamma(\alpha_N)}\frac{1}{\sqrt{2\pi\alpha_N}}\sqrt{\frac{\alpha_N}{\tilde{\gamma}_N\beta_N}}\left(1+\frac{1}{2\alpha_N}\frac{\alpha_N}{\beta_N\tilde{\gamma}_N}\,(x-K_N)^2\right)^{-(2\alpha_N+1)/2}, \end{aligned} \tag{43}$$

where $\mathrm{InvGamm}(x)$ *is the inverse Gamma distribution. Here, the parameters α_N, β_N, γ_N, and K_N are given in terms of set of measurements:*

$$\begin{aligned} \beta_N &= \beta_0 + \frac{1}{2}\sum_{n=1}^{N}\frac{[x_{n+1}-x_n(1-K_N\Delta t)]^2}{\Delta t} + \frac{1}{2\gamma_0}\,(K_N-K_0)^2\,, \\ \alpha_N &= \alpha_0 + \frac{N}{2}\,, \\ K_N &= -\frac{1}{\Delta t}\left(-1+\frac{\Delta t\sum_{n=1}^{N}x_{n+1}x_n + \frac{1-K_0\Delta t}{\gamma_0}}{\frac{1}{\gamma_0}+\Delta t\sum_{n=1}^{N}x_n^2}\right), \\ \frac{1}{\gamma_N} &= \frac{1}{\gamma_0} + \Delta t\sum_{n=1}^{N}x_n^2\,, \end{aligned} \tag{44}$$

where the hyper-parameters α_0, β_0, γ_0, and K_0, determine the a priori *information we have about the model's parameters. From the posterior distributions P_D and $P_{\kappa_x/\gamma}$ we obtain the empirical estimates $D^{(\mathrm{ex})}$ and $\kappa_x^{(\mathrm{ex})}$ as the mean values and variances with respect to them, namely*

$$\begin{aligned} D^{(\mathrm{ex})} &= \int dx\; xP_D(x) = \frac{\beta_N}{2(\alpha_N-1)}\,, \qquad \sigma^2_{D^{(\mathrm{ex})}} = \frac{\beta_N^2}{4(\alpha_N-1)^2(\alpha_N-2)}\,, \\ \frac{\kappa_x^{(\mathrm{ex})}}{\gamma} &= \int dx\; xP_{\kappa_x}(x) = K_N\,, \qquad \sigma^2_{\kappa_x/\gamma} = \frac{\gamma_N\beta_N}{\alpha_N-1}\,. \end{aligned} \tag{45}$$

Formulas for higher cumulants are also known. Notice that for $N = 0$, that is having no data, we obtain the mean values and variances directly in term of the hyperparameters. Thus, α_0, β_0, γ_0, and K_0 can be

naturally fixed by our theoretical values and original systematic and lab uncertainties, that is $D^{(\mathrm{th})} \pm \sigma_{D^{(\mathrm{th})}}$ *and* $\kappa_x^{(\mathrm{th})}/\gamma \pm \sigma_{\kappa_x^{(\mathrm{th})}/\gamma}$*, by using the formulas:*

$$\alpha_0 = 2 + \frac{(D^{(\mathrm{th})})^2}{\sigma^2_{D^{(\mathrm{th})}}}, \qquad \beta_0 = \frac{2D^{(\mathrm{th})}[(D^{(\mathrm{th})})^2 + \sigma^2_{D^{(\mathrm{th})}}]}{\sigma^2_{D^{(\mathrm{th})}}},$$
$$K_0 = \frac{\kappa_x^{(\mathrm{th})}}{\gamma}, \qquad \gamma_0 = \frac{\sigma^2_{\kappa_x^{(\mathrm{th})}/\gamma}}{2D^{(\mathrm{th})}}. \tag{46}$$

For instance, from table 2 we have that the theoretical value for the diffusion coefficient is $D^{(\mathrm{th})} = 0.208627 \pm XX\ \mu m^2\ s^{-1}$*. This allows us to fix the values* $\alpha_0 = XX$ *and* $\beta_0 = XX$*. For the theoretical value of the inverse relaxation time, we are more in the dark, as we do not know the trap stiffness just yet. Let us assume we have a previous raw estimate that gives* $\kappa/\gamma \sim XX$ *and we add a 10 percent of error, being fairly conservative. This fixes the values of* $K_0 = XX$ *and* $\tilde{\gamma}_0 = XX$*.*

Using Bayesian inference in one of the time series $\{x_n^{(m)}\}_{n=1}^N$*, say the one corresponding to the first experiment, of experiment I (see Table 2 for more details), we obtain the estimates for the parameters of the problem for different values of N, as reported in Table 5. This table illustrates how Bayesian inference with a good prior distribution is able to obtain fairly good estimates even for small values of N. From the best estimates in the table, the last row, we have that* $\gamma^{(\mathrm{ex})} = XX \pm XX\ \mathrm{pN\,ms\,}\mu\mathrm{m}^{-1}$*, which we use to estimate the trap stiffness,* $\kappa_x^{(\mathrm{ex})} = XX \pm XX\ \mathrm{pN}\,\mu\mathrm{m}^{-1}$*. Final estimates for the other experiments are given in Table 4.*

Bayesian inference provides all statistical information of the experimental parameters from the measured data, and is therefore able to provide unbiased estimators for them. Moreover, in case of having little data, a good prior information helps to obtain good estimates of the parameters. This method can be generalized to more than one dimension for any time interval Δt*.*

1.10. Measurement of non-conservative force fields

While the previous methods rely on either the forces being conservative, with significant simplification in case of the potential being quadratic, in many experimental instances, the forces are non-conservative. Although the drift and ACF methods can be applied to non-conservative forces, in the latter case by using cross-correlations, we briefly show how the method of FORMA can be adapted to this case [21], while details of the Bayesian method can be found in [22].

For clarity, we consider the two-dimensional case, the generalization to higher dimensions is straightforward. Here the overdamped Langevin equations reads

$$\dot{\boldsymbol{r}} = \frac{1}{\gamma}\boldsymbol{F}(\boldsymbol{r}) + \sqrt{2D}\boldsymbol{w}, \tag{47}$$

where $\boldsymbol{F}(\boldsymbol{r})$ *is the force field and* $\boldsymbol{w}$ *is the vector of independent white noise. If we do a Taylor expansion for* $F(\boldsymbol{r})$ *around, let us say* $\boldsymbol{r} = \boldsymbol{0}$*, we have that*

$$\boldsymbol{F}(\boldsymbol{r}) = \boldsymbol{F}_0 + \boldsymbol{J}_0 \cdot \boldsymbol{r} + O(\boldsymbol{r}^2), \tag{48}$$

where $\boldsymbol{F}_0 = \boldsymbol{F}(\boldsymbol{0})$ *is the force and* $\boldsymbol{J}_0 = \boldsymbol{J}(\boldsymbol{0})$ *the Jacobian at the point* $\boldsymbol{r} = \boldsymbol{0}$*. If the point* $\boldsymbol{r} = \boldsymbol{0}$ *were to be an equilibrium point that* $\boldsymbol{F}_0 = \boldsymbol{0}$*, which henceforth we will assume this to be the case, without loss of generality.*

Now, analogously to the one-dimensional case, if we discretize the Langevin equation (47)*, we obtain*

$$\boldsymbol{f}_n = \gamma\frac{\Delta \boldsymbol{r}_n}{\Delta t} = \boldsymbol{J}_0 \cdot \boldsymbol{r}_n + \sigma \boldsymbol{w}_n \tag{49}$$

where $\sigma = \sqrt{\frac{2D\gamma^2}{\Delta t}}$ *and* $\boldsymbol{w}_n$ *is a vector of independent Gaussian numbers with zero mean and unit variance. The result given by Eq.* (49) *can be understood as a multivariate linear regression model: given a set of pairs of data points* $\{(\boldsymbol{r}_n, \boldsymbol{f}_n)\}_{n=1}^N$*, after constructing the likelihood for* (49) *and maximising with respect to*

$\boldsymbol{J}_0$, *we obtain the corresponding Maximum Likelihood Estimator* $\boldsymbol{J}_0^\star$ *given by Moore-Penrose pseudo-inverse:*

$$\boldsymbol{J}_0^\star = \left[\boldsymbol{R}^T\boldsymbol{R}\right]^{-1}\boldsymbol{R}^T\boldsymbol{F} \tag{50}$$

where $\boldsymbol{R}$ *(usually called observation matrix) and* $\boldsymbol{F}$ *are* $N \times 2$ *matrices given by*

$$\boldsymbol{R} = \begin{pmatrix} \boldsymbol{r}_1^T \\ \vdots \\ \boldsymbol{r}_N^T \end{pmatrix}, \qquad \boldsymbol{F} = \begin{pmatrix} \boldsymbol{f}_1^T \\ \vdots \\ \boldsymbol{f}_N^T \end{pmatrix}. \tag{51}$$

From the MLE $\boldsymbol{J}_0^\star$ *we can obviously estimate the force as* $\boldsymbol{F}^\star = \boldsymbol{J}_0^\star \cdot \boldsymbol{r}$*. This result can be naturally split into a purely conservative and non-conservative parts, corresponding to the symmetric and antisymmetric decompositions of* $\boldsymbol{J}_0^\star = \boldsymbol{J}_c^\star + \boldsymbol{J}_r^\star$*, respectively. The symmetric part can be rewritten as*

$$\boldsymbol{J}_c^\star = \frac{1}{2}\left(\boldsymbol{J}_0^\star + \boldsymbol{J}_0^{\star T}\right) = \boldsymbol{R}(\theta^\star)\begin{pmatrix} -\kappa_1^\star & 0 \\ 0 & -\kappa_2^\star \end{pmatrix}\boldsymbol{R}^{-1}(\theta^\star), \tag{52}$$

with $\boldsymbol{R}$ *a rotation matrix and* $\kappa_1^\star$ *and* $\kappa_2^\star$ *the trap stiffness along the principal axes. The rotational part is in turn given by*

$$\boldsymbol{J}_c^\star = \frac{1}{2}\left(\boldsymbol{J}_0^\star - \boldsymbol{J}_0^{\star T}\right) = \begin{pmatrix} 0 & -\gamma\Omega^\star \\ \gamma\Omega^\star & 0 \end{pmatrix}, \tag{53}$$

with $\Omega^\star$ *being the angular frequency.*

1.11. Active calibration techniques

The calibration methods we have discussed so far are passive*, i.e. they are based on the determination of the trap stiffness from the stochastic motion of the particle in thermal equilibrium with the surrounding fluid within a harmonic potential. It is also possible to determine experimental parameters by* actively *applying an external perturbation to the system and then measuring its response.*

A simple active method consists of exposing a particle held by the tweezers to external uniform flow in the $x-$*direction with a known velocity* v_{fluid} *so that the mean drag force exerted on the bead is* $F_{drag} = -\gamma v_{fluid}$*. The drag force results in a mean displacement of the particle position* x *from the trap center* x_{trap}*, i.e.* $\Delta x = \langle x - x_{trap}\rangle$*, in such a way that in a steady state the balance between the drag force and the restoring optical force of the tweezers leads to*

$$\kappa = \frac{\gamma v_{fluid}}{\Delta x} \tag{54}$$

Eq. (54) allows to determine the trap stiffness κ *by measuring the mean particle displacement* Δx*, provided that the friction coefficient* γ *is known. In practice, it is easier to apply uniform flow by moving the sample at constant speed* v_{fluid} *[23], e.g. by means of a piezoelectric translation stage, and keeping the particle far away from the cell walls in order to avoid hydrodynamics interactions which change the value of friction coefficient* γ *with respect to the value given by the Stokes' law.*

Another active method which not only provides the value of the the trap stiffness but also the drag coefficient and the spatial conversion factor of x *into actual distances, can be implemented by sinusoidally moving the position* x_{stage} *of the sample stage while keeping the bead trapped by the tweezers at fixed* $x_{trap} = 0$ *[24], i.e.*

$$x_{stage}(t) = A\sin(2\pi f_{stage}t)\,. \tag{55}$$

The resulting flow velocity is $v_{stage}(t) = 2\pi f_{stage}A\cos(2\pi f_{stage}t)$*, thus the equation of motion for the particle in this case becomes*

$$\frac{dx(t)}{dt} - v_{stage}(t) = -2\pi f_{c,x}x(t) + \sqrt{2D}W_x(t), \tag{56}$$

where, as usual, $W_x(t)$ is a Gaussian white noise with zero mean, i.e. $\langle W_x(t)\rangle = 0$, and delta correlated in time, i.e. $\langle W_x(t)W_x(t')\rangle = \delta(t-t')$. Following the previous section, from Eqs. (55) and (56) we find that the PSD of the particle position is

$$P(f) = \frac{D}{\pi^2}\frac{1}{f^2+f_{c,x}^2} + \frac{A^2}{2\left(1+\frac{f_{c,x}^2}{f_{stage}^2}\right)}\delta\left(f-f_{stage}\right). \tag{57}$$

In Equation (57), the first term on the right-hand side accounts for the thermal contribution to the PSD, $P_T(f) = \frac{D/\pi^2}{f^2+f_{c,x}^2}$, and is equal to that given by Equation (Refer to Equation for passive PSD), while the second term corresponds to the mechanical response of the particle to the excitation frequency $f = f_{stage}$. Because the measurement time in an experiment is finite, $t_{msr} < \infty$, the Dirac-delta peak in Equation (57) becomes a spike with finite height $P_{stage} = P(f_{stage})$ and width Δf. If the total mesurement time is chosen to be an integer mutiple of the driving frequency of the stage, then the spike reduces to a single datum P_J at frequency $f_J = f_{\text{stage}}$ for some integer J, whereas $\Delta f = 2\delta f$, where δf corresponds to the frequency resolution of the PSD. In this case, the discrete version of Equation (58) for the $j-th$ data point is

$$P_j = \frac{D}{\pi^2}\frac{1}{f_j^2+f_{c,x}^2} + \frac{A^2 t_{msr}}{2\left(1+\frac{f_{c,x}^2}{f_j^2}\right)}\delta_{j,J}, \tag{58}$$

where $\delta_{j,J}$ represents the Kronecker delta. Therefore, by disregarding the single point (f_J, P_J), a fit $P_{fit}(f)$ into the one-sided Lorentzian function in Eq. (58) allows to compute the diffusion coefficient $D^{(1)}$ and the corner frequency $f_{c,x}$, from which the trap stiffness can be determined:

$$\kappa^{(1)} = \frac{2\pi f_{c,x} k_B T}{D^{(1)}}. \tag{59}$$

Note that, if x has not been yet converted into units of length, the values and units of $D^{(1)}$ and $\kappa^{(1)}$ are not correct. A further step using the active component of the sprectrum in Eq. (58) allows to get the calibration factor α of x into units of legth: $x \to \alpha x$, where α can have units of m/V or $m/pixel$ depending on whether the particle position was recorded with a quadrant photodiode, a position sensitive detector or a camera. The power contained in the triangular spike centered at $j = J$, $W^{exp} = \frac{1}{2}[P_J - P_{fit}(f_J)]2\delta f$, where $P_{fit}(f_J) = \frac{D^{(1)}/\pi^2}{f_J^2+f_{c,x}^2}$, and the theoretical value given in the in Equation (57), $W^{th} = \frac{A^2}{2\left(1+f_{c,x}^2/f_{stage}^2\right)}$, must be equal. Then, $\alpha^2 W_{exp} = W^{th}$, from which

$$\alpha = \frac{A}{\sqrt{2\left(1+\frac{f_{c,x}^2}{f_J^2}\right)[P_J - P_{fit}(f_J)]\delta f}}. \tag{60}$$

Hence, the corrected values with the right units of the trap stiffness and the friction coefficient are

$$\kappa = \frac{2\pi f_{c,x} k_B T}{\alpha^2 D^{(1)}}, \tag{61}$$

$$\gamma = \frac{k_B T}{\alpha^2 D^{(1)}}, \tag{62}$$

respectively.

An alternative to the aforementioned method when no translational stage but an acousto-optic deflector is available, is to move the position of the center of the trap, while keeping the sample cell at rest, i.e. $x_{stage} = 0$ and

$$x_{trap}(t) = A\sin(2\pi f_{trap} t). \tag{63}$$

In this case the motion of the trapped particle is described by the following Langevin equation

$$\frac{dx(t)}{dt} = -2\pi f_{c,x}\left[x(t) - x_{trap}(t)\right] + \sqrt{2D}W_x(t). \tag{64}$$

Note that here, unlike the case of an external flow, an effective oscillatory force $kx_{trap}(t) = kA\sin(2\pi f_{trap}t)$ is exerted on the trapped particle. The corresponding power spectral of the particle position is given in this case by

$$P(f) = \frac{D}{\pi^2}\frac{1}{f^2 + f_{c,x}^2} + \frac{A^2}{2\left(1 + \frac{f_{trap}^2}{f_{c,x}^2}\right)}\delta\left(f - f_{trap}\right). \tag{65}$$

while its discretized form is

$$P_j = \frac{D}{\pi^2}\frac{1}{f_j^2 + f_{c,x}^2} + \frac{A^2 t_{msr}}{2\left(1 + \frac{f_j^2}{f_{c,x}^2}\right)}\delta_{j,J}, \tag{66}$$

Thus, once the PSD of the particle position is computed, the calibration of α, κ and γ proceeds similar to the case of the oscillatory flow created by moving the stage, see Equations (59)-(62).
Active calibration methods can also be applied to less trivial situations, for instance for particles trapped in viscoleastic fluids [25, 26]. In such a case, the instantaneous drag force on the particle at time t is not simply given by $\gamma\frac{dx(t)}{dt}$ as in Equations (56) *and* (64)*, but it is related to the frequency-dependent rheological properties of the medium, which are a priori unkown. See Section Microrheology for further details about how to extract such physical quantities.*

1.12. Direct optical force measurement

As we have discussed, all the calibrations methods discussed thus far have a number of difficulties and limitations: assuming that the particle has a given size or shape, or even the beam shape, after recording the particles's position one indirectly infers the properties of the optical forces and those of the particle by non-linearly fitting the theory with experimental measurements.
It is possible, however, to overcome these limitations by measuring directly the force field, meaning that these direct measurements techniques can potentially be applied to living cells, particles of arbitrary shape and non-Gaussian beams [3, 27, 28].
Direct measurement of optical forces is based on recording the change of momentum between the in and outgoing light, since the exerted optical force is equal to the change in the momentum flux of the trapping light. More precisely, the idea works as follows: let $I(\theta, \varphi)$ be the intensity scattered into the director (θ, φ), given in spherical coordinates. Then, the momentum flux density $\dot{\boldsymbol{p}}$ of the outgoing light is

$$\dot{\boldsymbol{p}} = \frac{1}{c}I(\theta,\varphi)\begin{pmatrix}\sin\theta\cos\varphi\\ \sin\theta\sin\varphi\\ \cos\theta\end{pmatrix}. \tag{67}$$

The optical force acting on the particle corresponds to the difference between the total momentum flux of ingoing and outgoing light, where the incoming momentum flux is given by precisely the same formula but with opposite sign. The most relevant point of this method is that one should be able to detect all of the scattered light in the experiment. Further details of how this can be achieved experimentally can be found in Ref. [3].

1.13. Mathematical details on error analysis and fitting

Most of the calibration techniques described above are based on using a particular physical observable Ψ, either a dynamical observable or a stationary one, that depends on a single trajectory. Let us denote its experimental estimate coming from a single trajectory as $\Psi_m^{(\mathrm{ex})}(\alpha) \equiv \Psi_m^{(\mathrm{ex})}(\alpha, \{x_\ell^{(m)}\}_{\ell=1}^N)$. Here α may denote either a time dependence or a spatial one. For instance, in the potential method α represents the position associated to one of the bins in the histogram, while for the MSD α corresponds to the discrete time. We can then use the M experiments to calculate the empirical mean and the empirical covariance of

the physical observable Ψ. *These are:*

$$\overline{\Psi^{(\mathrm{ex})}}(\alpha) = \frac{1}{M}\sum_{m=1}^{M}\Psi_m^{(\mathrm{ex})}(\alpha)\,, \tag{68}$$

$$\Delta^{(\Psi)}_{\alpha,\beta} = \frac{1}{M-1}\sum_{m=1}^{M}\left[\Psi_m^{(\mathrm{ex})}(\alpha)-\overline{\Psi^{(\mathrm{ex})}}(\alpha)\right]\left[\Psi_m^{(\mathrm{ex})}(\beta)-\overline{\Psi^{(\mathrm{ex})}}(\beta)\right]+\epsilon^2_{\eta_1,\eta_2,\ldots}(\alpha)\,. \tag{69}$$

Notice that the expression for empirical covariance matrix $\Delta^{(\Psi)}_{\alpha,\beta}$ *in equation* (69) *has two terms. The first one corresponds to the experiment-to-experiment fluctuations that arise naturally due to the intrinsic randomness of the physical problem and, moreover, we have generally assumed that the experimental data may be correlated for different points* α *and* β. *The second term, denoted* $\epsilon^2_{\eta_1,\eta_2,\ldots}$, *captures the variances due to some known error in some variables* $(\eta_1,\eta_2,\ldots)$ *that are needed to compute* $\Psi_q^{(\mathrm{ex})}(\alpha)$ *as, for instance, uncertainties* $\delta\alpha$ *in the value of* α. *These type of errors can be estimated by standard techniques to propagate errors*[4] *[29].*

Once the set of empirical means and covariance matrix $\{\overline{\Psi^{(\mathrm{ex})}}(\alpha),\Delta^{(\Psi)}_{\alpha,\beta}\}$ *have been calculated, the following step is to fit them with the corresponding physical observable or model* $\Psi(\alpha;\vec{\theta})$ *in order to infer a family of unknown parameters* $\vec{\theta}=(\theta_1,\ldots,\theta_q)$ *of the model. There are several approaches to perform this task, probably the most popular are those based in least-square regressions (LSR), which defines the best estimates of the parameters as those that minimize the mean squared error*[5]. *In this tutorial, we will focus on a general least-squares method, so let us very briefly review this approach*[6]. *We then introduce the weighted* χ^2 *function as*

$$\chi^2(\vec{\theta}) = \sum_{\alpha,\beta=1}^{P}\left(\overline{\Psi^{(\mathrm{ex})}}(\alpha)-\Psi(\alpha;\vec{\theta})\right)R_{\alpha,\beta}\left(\overline{\Psi^{(\mathrm{ex})}}(\beta)-\Psi(\beta;\vec{\theta})\right), \tag{71}$$

where $R_{\alpha\beta}$ *is a symmetric semi-positive definite matrix, trying to capture correlation in the experimental dataset. When R is taken to be* $[\Delta^{(\Psi)}]^{-1}$ *this is the so-called generalised least-squares method or the correlated* χ*-squared method. The standard weighted least squared method is recovered when the off-diagonal terms of the empirical covariance are assumed to be zero so that* $[\Delta^{(\Psi)}]^{-1}_{\alpha\beta} = diag\left(1/\Delta^{(\Psi)}_{11},\ldots,1/\Delta^{(\Psi)}_{PP}\right)$. *If we do not have access to empirical errors one then performs the standard least squares method by assuming the matrix* $\Delta^{(\Psi)}$ *to be equal to the identity matrix. Either way, the main goal is to find the set of parameters* $\vec{\theta}^{(\star)}$ *that minimizes* $\chi^2(\vec{\theta})$. *In some cases, the inverse of the sample covariance matrix is an ill-posed problem and it is highly recommended to use the standard method of weighted least squares but including empirical covariance matrix in the error estimation of the parameters [5]. This is the approach we have used to estimate errors for the MSD and ACF methods.*

If the expression $\chi^2(\vec{\theta})$ *is functionally simple enough in the parameters, the minimization can be carried out analytically. A paradigmatic case corresponds when* $\Psi(\alpha;\vec{\theta})$ *is linear with respect to the model's parameters, that is*

$$\Psi(\alpha;\vec{\theta}) = \sum_{j=1}^{q}\theta_j\Phi_j(\alpha), \tag{72}$$

where $\{\Phi_j(\alpha)\}$ *is a set of functions, giving rise to the well stablished linear least square fitting. In some cases, a simple redefinition of variables can transform a non-linear fitting into a linear one, as, for instance,*

[4]Using propagation of errors, the contribution to the total variance by the errors in the uncorrelated variables $\eta_1,\eta_2,\ldots$ is

$$\epsilon^2_{\eta_1,\eta_2,\ldots}(\alpha)\approx\frac{1}{M}\sum_{m=1}^{M}\left[\left|\frac{\partial\Psi_m^{(\mathrm{ex})}(\alpha)}{\partial\eta_1}\right|^2\delta^2_{\eta_1}+\left|\frac{\partial\Psi_m^{(\mathrm{ex})}(\alpha)}{\partial\eta_2}\right|^2\delta^2_{\eta_2}+\ldots\right], \tag{70}$$

where δ_{η_1}, δ_{η_2}, ... are the errors associated to the corresponding variables.

[5]Less common, but very powerful methods, are the robust least-squares, including the least absolute regression (LAR) [30] and the Bisquare weights (BW) [31], both very useful to minimize the effect of outliers.

[6]A fantastic book that deals extremely well in these matters is the one of Peter Young [29]

in the potential method. On the other hand, when it is not possible to obtain explicit forms for $\vec{\theta}^{(\star)}$, one must rely on numerical minimizers, being the standard ones the Levenberg-Marquardt-Girard-Wynne-Morrison and the Trust-Region, implemented already in most of the standard computational packages for mathematical analysis, such as Python, MATLAB, Mathematica, and R. Notice, however, that the computational methods given in these packages do not normally allow to use the empirical covariance matrix to estimate the covariance matrix of the estimated parameters. In this case, it is recommended to use the packages provided in [5], which we also have implemente in this tutorial.

References

1. *A. Rohrbach, "Stiffness of optical traps: Quantitative agreement between experiment and electromagnetic theory," Phys. Rev. Lett.* ***95****, 168102 (2005).*
2. *P. H. Jones, O. M. Maragò, and G. Volpe,* Optical tweezers: Principles and applications *(Cambridge University Press, 2015).*
3. *G. Thalhammer, L. Obmascher, and M. Ritsch-Marte, "Direct measurement of axial optical forces," Opt. express* ***23****, 6112–6129 (2015).*
4. *H. Risken,* The Fokker-Planck equation *(Springer, 1996).*
5. *K. Fogelmark, M. A. Lomholt, A. Irbäck, and T. Ambjörnsson, "Fitting a function to time-dependent ensemble averaged data," Sci. reports* ***8****, 6984 (2018).*
6. *K. Berg-Sorensen and H. Flyvbjerg, "Power spectrum analysis for optical tweezers," Rev. Sci. Instrumen.* ***75****, 594–612 (2004).*
7. *P. Wu, R. Huang, C. Tischer, A. Jonas, and E.-L. Florin, "Direct measurement of the nonconservative force field generated by optical tweezers," Phys. review letters* ***103****, 108101 (2009).*
8. *D. Ryter and U. Deker, "Properties of the noise-induced spuriousdrift. i." J. Math. Phys.* ***21****, 2662–2665 (1980).*
9. *T. Brettschneider, G. Volpe, L. Helden, J. Wehr, and C. Bechinger, "Force measurement in the presence of brownian noise: Equilibrium-distribution method versus drift method," Phys. Rev. E* ***83****, 041113 (2011).*
10. *G. Volpe, L. Helden, T. Brettschneider, J. Wehr, and C. Bechinger, "Influence of noise on force measurements," Phys. review letters* ***104****, 170602 (2010).*
11. *A. W. Lau and T. C. Lubensky, "State-dependent diffusion: Thermodynamic consistency and its path integral formulation," Phys. Rev. E* ***76****, 011123 (2007).*
12. *R. Graham and A. Schenzle, "Stabilization by multiplicative noise," Phys. Rev. A* ***26****, 1676 (1982).*
13. *P. Sura, M. Newman, C. Penland, and P. Sardeshmukh, "Multiplicative noise and non-gaussianity: A paradigm for atmospheric regimes?" J. atmospheric sciences* ***62****, 1391–1409 (2005).*
14. *L. Pérez García, J. Donlucas Pérez, G. Volpe, A. V. Arzola, and G. Volpe, "High-performance reconstruction of microscopic force fields from Brownian trajectories," Nat. Commun.* ***9****, 5166 (2018).*
15. *R. Singh, D. Ghosh, and R. Adhikari, "Fast Bayesian inference of the multivariate Ornstein-Uhlenbeck process," Phys. Rev. E* ***98****, 012136 (2018).*
16. *S. Türkcan, A. Alexandrou, and J.-B. Masson, "A Bayesian inference scheme to extract diffusivity and potential fields from confined single-molecule trajectories." Biophys. J.* ***102****, 2288–2298 (2012).*
17. *M. U. Richly, S. Türkcan, A. Le Gall, N. Fiszman, J. Masson, N. Westbrook, K. Perronet, and A. Alexandrou, "Calibrating optical tweezers with Bayesian inference," Opt. Express* ***21****, 31578–31590 (2013).*
18. *M. El Beheiry, S. Türkcan, M. U. Richly, A. Triller, A. Alexandrou, M. Dahan, and J.-B. Masson, "A primer on the Bayesian approach to high-density single-molecule trajectories analysis," Biophys. J.* ***110****, 1209–1215 (2016).*
19. *S. Bera, S. Paul, R. Singh, D. Ghosh, A. Kundu, A. Banerjee, and R. Adhikari, "Fast Bayesian inference of optical trap stiffness and particle diffusion," Sci. Rep.* ***7****, 41638 (2017).*
20. *I. Pérez Castillo, G. Volpe, L. Pérez García, and A. V. Arzola, "Bayesian inference for estimating parameters of Brownian motion," preparation (2019).*
21. *L. P. García, J. D. Pérez, G. Volpe, A. V. Arzola, and G. Volpe, "High-performance reconstruction of microscopic force fields from brownian trajectories," Nat. communications* ***9****, 5166 (2018).*
22. *I. Pérez Castillo, G. Volpe, L. Pérez García, and A. V. Arzola, "Bayesian inference for estimating parameters of brownian motion," In preparation (2019).*
23. *R. M. Simmons, J. T. Finer, S. Chu, and J. A. Spudich, "Quantitative measurements of force and displacement using an optical trap," Biophys. journal* ***70****, 1813–1822 (1996).*
24. *S. F. Tolić-Nørrelykke, E. Schäffer, J. Howard, F. S. Pavone, F. Jülicher, and H. Flyvbjerg, "Calibration of optical tweezers with positional detection in the back focal plane," Rev. scientific instruments* ***77****, 103101 (2006).*
25. *M. Fischer and K. Berg-Sørensen, "Calibration of trapping force and response function of optical tweezers in viscoelastic media," J. Opt. A: Pure Appl. Opt.* ***9****, S239 (2007).*
26. *M. Fischer, A. C. Richardson, S. N. S. Reihani, L. B. Oddershede, and K. Berg-Sørensen, "Active-passive calibration of optical tweezers in viscoelastic media," Rev. Sci. Instruments* ***81****, 015103 (2010).*
27. *A. Farré and M. Montes-Usategui, "A force detection technique for single-beam optical traps based on direct measurement of light momentum changes," Opt. express* ***18****, 11955–11968 (2010).*
28. *M. Ritsch-Marte, F. Strasser, and G. Thalhammer, "Mapping out individual optical forces and torques of trapped particles by means of phase retrieval," in* Bio-Optics: Design and Application, *(Optical Society of America, 2019),*

pp. JW3A–2.
29. P. Young, Everything you wanted to know about data analysis and fitting but were afraid to ask *(Springer, 2015).*
30. Least Absolute Deviation Regression *(Springer New York, New York, NY, 2008), pp. 299–302.*
31. P. J. Huber, Robust Statistics*, Wiley series in probability and mathematical statistics (Wiley, 1981).*

Method	Key formulas	Comments
Potential	$\rho(x) = \rho_0 e^{-\frac{U(x)}{k_B T}}$	Useful for general potentials. Does not require fast acquisition, but it requires large datasets taken for long times $T >> \tau_{ot,x}$. When the potential is supposed to be harmonic, an analytical solution exists. Retrieves only κ_x.
Equipartition	$\kappa_x = \frac{k_B T}{\langle (x - x_{eq})^2 \rangle}$	The simplest and easiest method to implement. It is restricted to harmonic potentials and retrieves only κ_x. Does not require fast acquisition, but it requires large datasets taken for long times $T >> \tau_{ot,x}$. As it is defined via the square of the position, it results very sensitive to errors in the position detection.
MSD	$\mathrm{MSD}_x(\tau) = \frac{2k_B T}{\kappa_x}\left(1 - e^{-\frac{\lvert\tau\rvert}{\tau_{ot,x}}}\right)$	Retrieves κ_x and γ. It is very slow owing the large number of operations in the definition of the discrete MSD. There not exist an analytic solution for the fitting and the it has to be performed only with a selected dataset within some characteristic times of the trap. Care has to be taken when defining the errors for the MSD in short times since these points carry the highest relative error of the position detection and have very small values that can introduce outliers in the fitting.
ACF	$C_x(\tau) = \frac{k_B T}{\kappa_x} e^{-\frac{\lvert\tau\rvert}{\tau_{ot,x}}}$	Retrieve κ_x and γ. It is much faster than the MSD since there exist fast routines to compute the autocorrelation function. There exist an analytical solution and the fitting has to be performed with a selected dataset within some characteristic times of the trap.
PSD	$P_x(f) = \frac{1}{2\pi^2}\frac{D}{f_{c,x}^2 + f^2}$	Retrieve κ_x and γ. Can get rid of common signals of noise and aliasing usually seen in the high frequency region. The estimate of κ_x does not depend on any position calibration.
FORMA	$\mathcal{L}(\{x_n\}_{n=1}^N \lvert \{x_{0n}\}_{n=1}^N, \kappa_x/\gamma, D)$	It can retrieve κ_x and γ. It is fast since does not require a large amount of data and is defined by a simple analytical expression. The estimate of κ_x does not depend on any position calibration. The estimate of γ is very sensitive to the position detection. Able to reconstruct forces of arbitrary shape, including non-conservative when the analysis is extended to two-dimensions.
Bayesian inference	$P(\kappa_x/\gamma, D) = \frac{\mathcal{L}(\{x_n\}_{n=1}^N \lvert \{x_{0n}\}_{n=1}^N, \kappa_x/\gamma, D) P_0(\kappa_x/\gamma, D)}{Z}$	??

Method		**Experiment I** (2.3 mW) IS / AS	**Experiment II** (6.0 mW) IS / AS	**Experiment III** (9.2 mW) IS / AS
Potential	κ	13.58 ± 0.23 / 13.56 ± 0.22	34.52 ± 0.22 / 34.57 ± 0.22	55.97 ± 0.38 / 56.00 ± 0.35
Equipartition	κ	- - - - - - - - / 13.62 ± 0.37	- - - - - - - - / 34.93 ± 0.64	- - - - - - - - / 56.29 ± 1.14
MSD	κ	13.61 ± 0.04 / - - - - - - - -	35.02 ± 0.1 / - - - - - - - -	56.46 ± 0.15 / - - - - - - - -
	γ	18.73 ± 0.2 / - - - - - - - -	18.85 ± 0.21 / - - - - - - - -	18.88 ± 0.16 / - - - - - - - -
	D	13.61 ± 0.04 / - - - - - - - -	35.02 ± 0.1 / - - - - - - - -	56.46 ± 0.15 / - - - - - - - -
ACF	κ	13.61 ± 1.89 / 13.59 ± 0.18	34.70 ± 1.57 / 34.78 ± 0.25	55.45 ± 1.47 / 55.54 ± 0.47
	γ	18.8 ± 2.79 / 18.70 ± 0.28	18.57 ± 0.92 / 18.70 ± 0.19	18.25 ± 0.60 / 18.35 ± 0.23
	D	13.61 ± 0.04 / - - - - - - - -	35.02 ± 0.1 / - - - - - - - -	56.46 ± 0.15 / - - - - - - - -
PSD	κ	13.55 ± 0.31 / 13.52 ± 0.5	34.59 ± 0.58 / 34.5 ± 0.89	55.38 ± 0.82 / 55.2 ± 1.25
	γ	18.42 ± 0.08 / 18.36 ± 0.31	18.35 ± 0.09 / 18.3 ± 0.31	18.3 ± 0.09 / 18.24 ± 0.31
	D	13.61 ± 0.04 / - - - - - - - -	35.02 ± 0.1 / - - - - - - - -	56.46 ± 0.15 / - - - - - - - -
FORMA	κ	- - - - - - - - / 13.74 ± 0.12	- - - - - - - - / 35.76 ± 0.22	- - - - - - - - / 58.44 ± 0.29
	γ	- - - - - - - - / 21.8 ± 0.24	- - - - - - - - / 22.73 ± 0.02	- - - - - - - - / 23.58 ± 0.02
	D	13.61 ± 0.04 / - - - - - - - -	35.02 ± 0.1 / - - - - - - - -	56.46 ± 0.15 / - - - - - - - -
Bayesian	κ	13.75 ± 0.12	35.49 ± 0.21	57.51 ± 0.29
inference	γ	21.8 ± 0.02	22.73 ± 0.02	23.57 ± 0.02
	D	13.61 ± 0.04 / - - - - - - - -	35.02 ± 0.1 / - - - - - - - -	56.46 ± 0.15 / - - - - - - - -

Table 4. Experimental results. Experimental values for the stiffness obtained when Experiments I, II and III are analyzed according to the various methods in pN μm^{-1} and of the friction coefficient in pN msμm^{-1}. Each method provides the stiffness of the optical tweezer and may also provide the Stoke's drag coefficient of the particle in the fluid. The same particle with radius $a = 1.03$ μm was used in three experiments with three different powers in the optical tweezer (see Table 2 for more details about the experiment). For comparison, the theoretical value of the friction coefficient is $\gamma^{(\mathrm{th})} = 19.4 \pm XX$ pN ms μm^{-1}. REVISAR DIFFERENCIA IS/AS Y REVISAR ERROR DE MSD

N	$D^{(\mathrm{ex})} \pm \sigma_{D^{(\mathrm{ex})}}$ (μm^{2}s^{-1})	$\kappa_x^{(\mathrm{ex})}/\gamma \pm \sigma_{\kappa_x/\gamma}$ (s^{-1})
10^2	0.38 ± 0.05	149.9 ± 3.0
10^4	0.383 ± 0.005	150.0 ± 2.9
2×10^5	0.395 ± 0.001	154.74 ± 1.76

Table 5. Bayesian inference analysis. Resulting values for the estimates of experiment I for various values of N, starting with initial values of $\alpha_0 = 4$, $\beta_0 = 3$, $K_0 = 150$ and $\tilde{\gamma}_0 = 1$.